

Synchronization of multiple rigid body systems: a survey

Xin Jin,^{1, a)} Daniel W. C. Ho,² and Yang Tang^{3, b)}

¹⁾*The Research Institute of Intelligent Complex Systems, Fudan University, Shanghai 200433, China*

²⁾*The Department of Mathematics, City University of Hong Kong, Hong Kong, China*

³⁾*The Key Laboratory of Smart Manufacturing in Energy Chemical Process, East China University of Science and Technology, Shanghai 200237, China*

(*Electronic mail: yangtang@ecust.edu.cn)

(*Electronic mail: madaniel@cityu.edu.hk)

(*Electronic mail: jx_9810@163.com)

(Dated: 29 August 2023)

The multi-agent system has been a hot topic in the past few decades owing to its lower cost, higher robustness, and higher flexibility. As a particular multi-agent system, the multiple rigid body system received a growing interest for its wide applications in transportation, aerospace, and ocean exploration. Due to the non-Euclidean configuration space of attitudes and the inherent nonlinearity of the dynamics of rigid body systems, synchronization of multiple rigid body systems is quite challenging. This paper aims to present an overview of the recent progress in synchronization of multiple rigid body systems from the view of two fundamental problems. The first problem focuses on attitude synchronization, while the second one focuses on cooperative motion control in that rotation and translation dynamics are coupled. Finally, a summary and future directions are given in the conclusion.

The distributed sensing, decision-making, and cooperative control of multi-agent systems has been thoroughly investigated in the fields such as sensor networks, social networks, distributed computing, and robotics in the past decades. Recently, multiple rigid body systems as a particular kind of multi-agent system attracted a lot of interest from researchers owing to its potential applications in aerospace engineering, unmanned vehicles, and industrial robotics. This work aims to give a review of the recent research progress in synchronization of multiple rigid body systems from the aspects of two fundamental problems, which are attitude synchronization and coordination control of multiple rigid body systems. The basic kinematic and dynamic model of describing rigid body systems are introduced, and the important results as well as the comparisons are given. Finally, several future topics are outlined.

I. INTRODUCTION

The last decades have witnessed a significant progress in consensus studies of multi-agent networks¹⁻⁷. Through local knowledge and information interaction, agents can cooperatively complete a complicated task with lower cost, higher flexible, and higher robustness^{8,9}. As a kind of particular case in multi-agent systems, multiple rigid body systems have stronger engineering backgrounds in the fields such

as robotics¹⁰, satellites¹¹, and unmanned aerial vehicles¹². For example, with the rapid development of the perception ability of autonomous systems and artificial intelligence, in aerospace engineering, the coordination of a group of small or nano-satellites can deliver a comparable or even stronger capability compared with a monolithic satellite in completing the complex space mission such as distributed observation, on-orbit assembly, and asteroid defense^{13,14}. Typically, an inspection mission for coordinated observing a spacecraft target with a group of nano-satellites is shown in Fig. 1¹¹.

The rigid body can be considered as an idealization model of a body that does not deform or change shape under external forces¹⁵. The motion of rigid body is composed of the rotational and translational motion. From this point of view, synchronization of multiple rigid body systems in the literature can be divided into two categories. The one is attitude consensus which focuses on the rotational motion, while the other focuses on the coordinated motion control in which the rotational and translational motion are coupled together. Note that the "synchronization" and the similar noun "consensus" are usually regarded as exchangeable concepts in the literature, which have a common intension. Thus, we use these two words with no distinction in this paper.

For the rotational motion, the attitude representation of a rigid body can be classified into parameterized representations and rotation matrices. The parameterized representations include Euler angles¹⁶, Rodrigues parameters¹⁷, Modified Rodrigues parameters (MRPs)¹⁸, and unit quaternions¹⁹. Euler angles are widely used in the formation control of aerial vehicles and quadrotors based on linearized models²⁰. Note that the underlying space of rotation matrices $\mathbb{SO}(3)$ is non-diffeomorphic to any Euclidean spaces²¹. Euler angles and modified Rodrigues parameters (MRPs) evolving on Euclidean spaces only achieve local convergence due to the singularity problem²². Several works studied the attitude synchronization problem based on the unit quaternion

^{a)}Xin Jin was with the Key Laboratory of Smart Manufacturing in Energy Chemical Process, Ministry of Education, East China University of Science and Technology, Shanghai 200237. Now he is with the Research Institute of Intelligent Complex Systems, Fudan University, Shanghai, China.

^{b)}Corresponding author: Yang Tang.

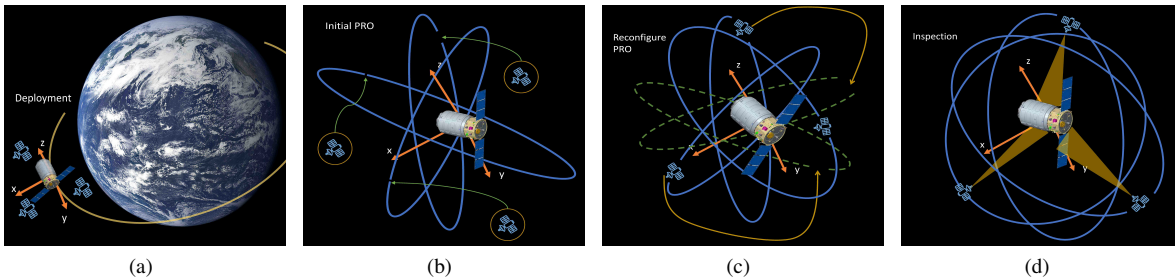


FIG. 1. An inspection mission with nano-satellites. (a). Deployment of three satellites around the target spacecraft. (b). Initialization of three satellites into stable relative orbits. (c). Reconfiguration of three satellites to observe a different area on the target. (d). Coordinated pointing control for observing the target spacecraft¹¹.

since it can globally represent the attitude. Nevertheless, it may suffer from the unwinding phenomenon due to the non-uniqueness of describing attitudes²¹. Hence, to overcome this problem, a hybrid feedback control approach has been utilized to design the controller, which can achieve the global attitude synchronization²³.

The rotation matrix is the only global and unique attitude representation, which completely represents the attitude. Motivated by this fact, a substantial amount of literature has been devoted to the investigation of attitude consensus based on rotation matrices^{24–26}. However, due to the geometric topological constraints, there is no continuous time-invariant feedback which can achieve the global attitude synchronization²⁷. Therefore, many studies have focused on considering the almost global attitude synchronization^{28,29} and see the references therein. It is noteworthy that, in some scenarios, the incompleteness or reduced attitude consensus has a more relevant practical application such as coordinated pointing of nano-satellite³⁰. The completed attitude consensus and incompleteness consensus can be both considered in a unified framework on S^n , $n = 2, 3$ ³¹. It should be noted that the synchronization problem on S^n attracts many interests from different disciplines, including coupled oscillators^{32,33}, complex networks^{34–36}, and quantum mechanics^{37–39}. More generally, the underlying space S^2 , S^3 , and $\mathbb{SO}(3)$ can be considered as a Riemannian manifold⁴⁰. Due to the geometric topology constraint, the consensus protocol is quite difficult to design and the convergence domain is hard to be determined analytically on nonlinear spaces. Recently, there are some novel approaches dealing with the consensus problem on different Riemannian manifolds such as gradient flow methods^{41,42}, lifting methods⁴³, and matrix decomposition methods⁴⁴.

Rigid body systems' rotational and translational motions are usually coupled in dynamic models. A rigid body dynamic model is challenging to be obtained precisely in practical applications, especially when it contains unknown dynamics and environmental disturbances⁴⁵. The Euler-Lagrange equation is equivalent to Newton's laws of motion in classical mechanics. It is an effective method to describe the rigid body dynamics when the force vectors are particularly complicated¹⁵. In the past few decades, the coordination control of Euler-Lagrange systems has been widely studied in the literature under undirected graphs⁴⁶ and directed graphs^{47–49},

respectively. Lately, motivated by the fact that communication among agents is unreliable in real applications, the coordination control of networked Euler-Lagrange systems is considered with time-delays⁵⁰, packet dropouts⁵¹, and sampled-data mechanism⁵². In addition, as a particular case of non-periodic sampled-data setting, the event-triggered coordination control has also been extensively studied for Euler-Lagrange systems to reduce the communication cost^{53,54}.

The most of results on the coordination control of Euler-Lagrange systems are based on the fundamental properties of Euler-Lagrange dynamics such as anti-symmetry and parameterized linearity, which are quite ideal. For example, when considering the motion of a rigid body on a special Euclidean group $\mathbb{SE}(3)$, the anti-symmetric property of Euler-Lagrange dynamics may not be guaranteed⁵⁵. Extensive research has been conducted on the coordinated motion control on $\mathbb{SE}(3)$ due to its theoretical challenges in handling the nonlinear configuration space⁵⁶ and the switching topologies⁵⁷.

Overall, synchronization of multiple rigid body systems have been thoroughly investigated in the past decades and have attracted a growing interest for researchers in theoretical research as well as in practical applications. Up to our knowledge, very few works give a comprehensive literature review for synchronization of multiple rigid body systems. Compared with the recent survey on attitude consensus of multiple spacecraft⁵⁸, we further consider a more general multiple rigid body model where the rotational dynamics and translational dynamics may couple together.

The remaining part of this paper proceeds as follows. Section II presents the notation and preliminary knowledge, including graph theory, attitude representations, rigid body kinematics, and rigid body dynamics. Sections III and IV show the representative results of attitude synchronization and coordination control of multiple rigid body systems. The conclusion is drawn in Section V finally.

II. PRELIMINARIES

A. Notations

\mathbb{R}^N and $\mathbb{R}^{N \times N}$ represent the Euclidean vector space and real matrix space, where N is a positive integer number.

\mathbb{N}^+ denotes the positive integer numbers. \mathbb{R}^+ represents the positive real numbers. For a vector $\mathbf{x} = [x_1, \dots, x_N]^\top \in \mathbb{R}^N$, $\|\mathbf{x}\|$ denotes the Euclidean norm, which is defined as $\|\mathbf{x}\| = \sqrt{x_1^2 + x_2^2 + \dots + x_N^2}$. $\mathbf{0}_3$ denotes a zero vector in \mathbb{R}^3 . $\bar{\lambda}(\mathbf{A})$ and $\underline{\lambda}(\mathbf{A})$ denote the maximum and minimum eigenvalue of the matrix \mathbf{A} , respectively. $\text{tr}(\mathbf{A})$ represents the trace of matrix \mathbf{A} . $|\mathcal{D}|$ denotes the number of elements in \mathcal{D} . The set $\mathbb{SO}(3)$ is a special orthogonal group and the set $\mathfrak{so}(3) = \{\mathbf{X} \in \mathbb{R}^{3 \times 3} : \mathbf{X}^\top = -\mathbf{X}\}$. The operators $(\cdot)^\wedge$ and $(\cdot)^\vee$ represent a mapping between the vector $\mathbf{x} = [x_1, x_2, x_3]^\top$ and the skew symmetric matrix $\mathbf{X} = \begin{bmatrix} 0 & -x_3 & x_2 \\ x_3 & 0 & -x_1 \\ -x_2 & x_1 & 0 \end{bmatrix}$, where $\mathbf{x}^\wedge = \mathbf{X}$ and $\mathbf{x} = \mathbf{X}^\vee$.

The sign function is defined as $\text{sgn}(x) = \begin{cases} 1 & x > 0 \\ 0 & x = 0 \\ -1 & x < 0 \end{cases}$.

B. Graph Theory

We first introduce some basic concepts in graph theory. Let $\mathcal{G} = \mathcal{G}\{\mathcal{V}, \mathcal{E}\}$ denote a topology graph, in which $\mathcal{V} = \{1, \dots, N\}$ represents a node set, and $\mathcal{E} \subseteq \mathcal{V} \times \mathcal{V}$ represents an edge set. The edge denoted as $(i, j) \in \mathcal{E}$ means that the node i is the node j 's neighbor. In other words, node j can receive node i 's message. All the neighbors of node i forms a set denoted as $\mathcal{N}_i = \{j \in \mathcal{V} : (j, i) \in \mathcal{E}\}$. For one undirected graph, if $(i, j) \in \mathcal{E}$, then $(j, i) \in \mathcal{E}$. A graph is connected if there exists a link between any two nodes. Let an adjacency matrix $\mathcal{A} = [a_{ij}] \in \mathbb{R}^{N \times N}$ associate with the graph \mathcal{G} , where $a_{ij} > 0$ if the node j is the node i 's neighbor and zero otherwise. We suppose $a_{ii} = 0$, which means that the self-connection is excluded here. The Laplacian matrix is denoted by $\mathcal{L} = [l_{ij}] \in \mathbb{R}^{N \times N}$. The diagonal elements l_{ii} of the Laplacian matrix are the in-degree of node i , which can be calculated as $\sum_{j=1}^N a_{ij}$, and the non-diagonal elements are defined as $l_{ij} = -a_{ij}, i \neq j$.

Since the topology graph can be time-varying in practical multi-agent systems, we introduce some definitions of switching topologies. Denote all the possible topologies of the graph \mathcal{G} as $\mathcal{G}_1, \mathcal{G}_2, \dots, \mathcal{G}_M$. Define a continuous piecewise constant switching signal as $\sigma(t) : [0, \infty) \rightarrow \{1, 2, \dots, M\}$. Let a dwell time $\tau_D > 0$ be as a lower bound between any two consecutive switching times, which are the switching instances $\{\tau_k \mid k = 1, 2, \dots\}$ satisfying

$$\inf_k (\tau_{k+1} - \tau_k) \geq \tau_D. \quad (1)$$

The union graph of $\mathcal{G}_{\sigma(t)}$ during the time interval $[t_1, t_2]$ is defined as

$$\mathcal{G}([t_1, t_2]) = \bigcup_{t \in [t_1, t_2]} \mathcal{G}_{\sigma(t)} = \left(\mathcal{V}, \bigcup_{t \in [t_1, t_2]} \mathcal{E}_{\sigma(t)} \right),$$

where $t_1 < t_2 \leq +\infty$. A wild assumption of switching topology is called jointly connected, which is defined as follows.

Definition 1 The switching topology $\mathcal{G}_{\sigma(t)}$ is jointly connected if there exists a constant $T > 0$ such that the union graph $\mathcal{G}[t, t+T]$ is connected for any $t \geq 0$.

C. Attitude representations and kinematics

Let \mathcal{F}_w denote the world frame and \mathcal{F}_i the local body frame of the rigid body i , where $i = 1, \dots, N$. The attitude of each rigid body i in the world frame \mathcal{F}_w is denoted by $\mathcal{R}_i \in \mathbb{SO}(3)$. Some examples of attitude representations and their kinematics are summarized in the following content. The global and unique property of attitude representations are summarized in Table I.

1. Rotation matrices

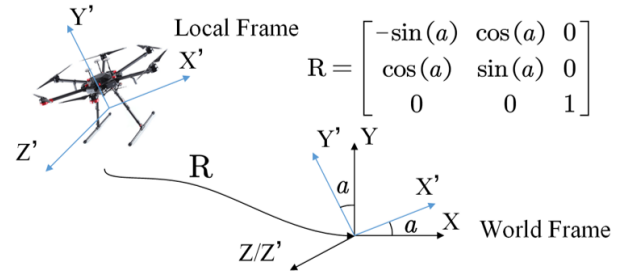


FIG. 2. Rotation between the local and world frame.

The rotation matrix is a linear transformation, which describes the rotation between the local frame and the world frame as shown in Fig. 2. All the rotation matrices form a special rotation group as follows,

$$\mathbb{SO}(3) = \left\{ \mathcal{R}_i \in \mathbb{R}^{3 \times 3} \mid \det \mathcal{R}_i = 1, \mathcal{R}_i \mathcal{R}_i^\top = \mathcal{R}_i^\top \mathcal{R}_i = \mathbf{I}_3 \right\}. \quad (2)$$

Based on the rotation matrix, the attitude kinematics of the i th rigid body is governed by

$$\dot{\mathcal{R}}_i = \mathcal{R}_i \boldsymbol{\omega}_i^\wedge, \quad i \in \mathcal{N}, \quad (3)$$

where $\mathcal{R}_i \in \mathbb{SO}(3)$, and $\boldsymbol{\omega}_i \in \mathbb{R}^3$ is the angular velocity.

TABLE I. Properties of attitude representations¹⁹.

Attitude representations	Global	Unique
Euler angles	No	No
Rodrigues parameters	No	No
Modified Rodrigues parameters	No	No
Quaternions	Yes	No
Rotation matrices	Yes	Yes

2. Axis-angle representations

Let $\mathbf{x}_i \in \mathbb{R}^3$ denote the axis-angle attitude representation of each rigid body i , which can be obtained by

$$\begin{aligned}\mathbf{x}_i^\wedge &= \log \mathcal{R}_i \\ &= \theta_i \mathbf{u}_i^\wedge,\end{aligned}\quad (4)$$

where $\log : \mathbb{SO}(3) \rightarrow \mathfrak{so}(3)$ is the logarithm map, $\theta_i \in [0, \pi]$ is the rotation angle with respect to the rotation axis $\mathbf{u}_i \in \mathbb{R}^3$.

More specifically,

$$\mathbf{u}_i^\wedge = \frac{1}{2 \sin(\theta_i)} (\mathcal{R}_i - \mathcal{R}_i^\top) \quad (5)$$

and

$$\cos(\theta_i) = \frac{\text{tr}(\mathcal{R}_i) - 1}{2}. \quad (6)$$

Note that the axis-angle vector is a global attitude representation, however, a pair of axis-angles corresponds to the same attitude at the point when $\theta_i = \pi$.

Based on the axis-angle representation, the attitude kinematics is given by²⁸ in the following,

$$\dot{\mathbf{x}}_i = \mathbf{J}_{\mathbf{x}_i} \boldsymbol{\omega}_i. \quad (7)$$

The Jacobian matrix $\mathbf{J}_{\mathbf{x}_i}$ is defined as

$$\begin{aligned}\mathbf{J}_{\mathbf{x}_i} &= \mathbf{I}_3 + \frac{\theta_i \mathbf{u}_i^\wedge}{2} + \left(1 - \frac{\theta_i}{2} \cot \frac{\theta_i}{2}\right) (\mathbf{u}_i^\wedge)^2 \\ &= \mathbf{J}_{\mathbf{x}_i}^\wedge + \frac{\theta_i \mathbf{u}_i^\wedge}{2},\end{aligned}\quad (8)$$

where $\mathbf{J}_{\mathbf{x}_i}^\wedge = \mathbf{I}_3 + \left(1 - \frac{\theta_i}{2} \cot \frac{\theta_i}{2}\right) (\mathbf{u}_i^\wedge)^2$ is the symmetric matrix. We know that if $\theta_i \in [0, \pi]$, the Jacobian matrix is positively definite, i.e., $\mathbf{x}_i^\top \mathbf{J}_{\mathbf{x}_i} \mathbf{x}_i > 0$ for all $\mathbf{x}_i \neq \mathbf{0}$, $\mathbf{x}_i \in \mathbb{R}^3$. When $\theta_i = 0$, $\mathbf{J}_{\mathbf{x}_i}^\wedge = \mathbf{I}_3$. In addition, we can get the geometric property of the Jacobian matrix in which the second and the third term are perpendicular to \mathbf{x}_i , i.e., $\mathbf{x}_i^\top \mathbf{J}_{\mathbf{x}_i} = \mathbf{x}_i^\top$.

3. Rodrigues parameters

Let $\mathbf{y}_i \in \mathbb{R}^3$ denote the Rodrigues parameter attitude representation of each rigid body i , which is given by

$$\mathbf{y}_i = \tan \frac{\theta_i}{2} \mathbf{u}_i, \quad (9)$$

where \mathbf{u}_i and θ_i are calculated by (5) and (6). Note that the Rodrigues parameters have singularities when the rotation angle $\theta_i = \pm\pi$. The attitude kinematics based on the Rodrigues parameters is given by

$$\dot{\mathbf{y}}_i = \frac{1}{2} \mathbf{h}_i(\mathbf{y}_i) \boldsymbol{\omega}_i, \quad (10)$$

where $\mathbf{h}_i(\mathbf{y}_i) = \mathbf{I}_3 + \mathbf{y}_i^\wedge + \mathbf{y}_i \mathbf{y}_i^\top$.

4. Modified Rodrigues parameters

Let $\boldsymbol{\sigma}_i \in \mathbb{R}^3$ denote the modified Rodrigues parameter of i th rigid body, which is given by

$$\boldsymbol{\sigma}_i = \tan \frac{\theta_i}{4} \mathbf{u}_i, \quad (11)$$

where \mathbf{u}_i and θ_i are consistent with (9). The Modified Rodrigues parameters also have singularity problems when $\theta_i = \pm 2\pi$. The attitude kinematics based on the Modified Rodrigues parameters is given by

$$\dot{\boldsymbol{\sigma}}_i = \mathbf{G}(\boldsymbol{\sigma}_i) \boldsymbol{\omega}_i, \quad i \in \mathcal{N}, \quad (12)$$

where $\mathbf{G}(\boldsymbol{\sigma}_i) = \frac{1}{2} \left(\frac{1 - \boldsymbol{\sigma}_i^\top \boldsymbol{\sigma}_i}{2} \mathbf{I}_3 + \boldsymbol{\sigma}_i^\wedge + \boldsymbol{\sigma}_i \boldsymbol{\sigma}_i^\top \right) \in \mathbb{R}^{3 \times 3}$. The matrix $\mathbf{G}(\boldsymbol{\sigma}_i)$ satisfies $\mathbf{G}(\boldsymbol{\sigma}_i) \mathbf{G}(\boldsymbol{\sigma}_i)^\top = \left(\frac{1 + \boldsymbol{\sigma}_i^\top \boldsymbol{\sigma}_i}{4} \right)^2 \mathbf{I}_3$ ²¹.

5. Unit quaternions

Let \mathbf{q}_i denote the unit quaternion of i th rigid body, which is defined as

$$\mathbf{q}_i = \begin{bmatrix} \eta_i \\ \boldsymbol{\epsilon}_i \end{bmatrix} \in \mathbb{S}^3, \quad (13)$$

where $\mathbb{S}^3 = \{(\eta_i, \boldsymbol{\epsilon}_i) \in \mathbb{R} \times \mathbb{R}^3 : \eta_i^2 + \boldsymbol{\epsilon}_i^\top \boldsymbol{\epsilon}_i = 1\}$, $\eta_i \in \mathbb{R}$ is a scalar part, and $\boldsymbol{\epsilon}_i \in \mathbb{R}^3$ is a vector part. Each unit quaternion $\mathbf{q}_i \in \mathbb{S}^3$ has the inverse $\mathbf{q}_i^{-1} = (\eta_i, -\boldsymbol{\epsilon}_i)$. Note that a pair of antipodal unit quaternions $\pm \mathbf{q}_i \in \mathbb{S}^3$ corresponds to the same attitude $\mathcal{R}_i \in \mathbb{SO}(3)$. The quaternion kinematic equation for agent i satisfies

$$\dot{\mathbf{q}}_i = \frac{1}{2} \begin{bmatrix} -\boldsymbol{\epsilon}_i^\top \\ \eta_i \mathbf{I}_3 + \boldsymbol{\epsilon}_i^\wedge \end{bmatrix} \boldsymbol{\omega}_i. \quad (14)$$

D. Parameterized attitude representations

The attitude representations in \mathbb{R}^3 are also called parameterized attitude representations. In fact, the parameterized attitude representations can be considered as coordinates in a chart, which covers an open ball around the identity matrix on $\mathbb{SO}(3)$ ⁵⁷. To make this point clear, a diffeomorphism mapping is used to give a unified definition for the parameterized attitudes⁵⁹.

Let $f : \mathcal{B}_r(\mathbf{I}) \subset \mathbb{SO}(3) \rightarrow \mathcal{B}_{r',3}(0) \subset \mathbb{R}^3$ be defined as a diffeomorphism mapping from $\mathbb{SO}(3)$ to \mathbb{R}^3 , where $\mathcal{B}_r(\mathbf{I}) = \{\mathcal{R} \in \mathbb{SO}(3) : d(\mathcal{R}, \mathbf{I}) < r\}$ is an open geodesic ball around the identity matrix in $\mathbb{SO}(3)$ with radius $r \leq \pi$, $\mathcal{B}_{r'}(\mathbf{0}) = \{\mathbf{x} \in \mathbb{R}^3 : \|\mathbf{x}\| < r'\}$ is an open ball around point $\mathbf{0}$ in \mathbb{R}^3 . If $r = \pi$, then $\mathcal{B}_r(\mathbf{I})$ covers $\mathbb{SO}(3)$ almost globally, i.e., the set $\mathbb{SO}(3) - \mathcal{B}_\pi(\mathbf{I})$ has measure zero. In addition, if $r \leq \frac{\pi}{2}$, $\mathcal{B}_r(\mathbf{I})$ is convex. Then, a general form of f can be given as $f(\mathcal{R}) = g(\theta(\mathcal{R})) \mathbf{u}(\mathcal{R})$, where $\theta(\mathcal{R})$ is the geodesic distance between

TABLE II. Local attitude representations⁵⁷

Coordinates	$f = g(\boldsymbol{\theta})\mathbf{u}$	r	r'
Axis-angles	$g(\boldsymbol{\theta}) = \theta$	π	π
Rodrigues parameters	$g(\boldsymbol{\theta}) = \tan(\frac{\theta}{2})$	π	$+\infty$
Modified Rodrigues parameters	$g(\boldsymbol{\theta}) = \tan(\frac{\theta}{4})$	π	1
$(\mathcal{R} - \mathcal{R}^\top)^\vee$	$g(\boldsymbol{\theta}) = \sin(\theta)$	$\frac{\pi}{2}$	1
Unit quaternions (Vector part)	$g(\boldsymbol{\theta}) = \sin(\frac{\theta}{2})$	π	1

\mathbf{I} and \mathcal{R} denoted as $d(\mathbf{I}, \mathcal{R}) = \theta$, $\mathbf{u}(\mathcal{R}) \in \mathbb{S}^2$ is a unit vector which represents the rotation axis of \mathcal{R} , $g(\cdot) : (-r, r) \rightarrow \mathbb{R}$ is an odd and strictly increasing function such that f is a diffeomorphism. Note that $r \leq \pi$ is the largest radius such that f is a diffeomorphism. $\theta(\mathcal{R})$, $\mathbf{u}(\mathcal{R})$ can be obtained using the logarithm map in (5) and (6).

Figure 3 illustrates the geometric configuration spaces of $\mathbb{SO}(3)$ and the open ball $\mathcal{B}_\pi(\mathbf{0}_3)$. Figure 3(a) shows a diffeomorphism of $\mathbb{SO}(3)$, which is a solid closed ball $\mathcal{B}_\pi(\mathbf{I}_3) = \{\mathcal{R} \in \mathbb{SO}(3) : d(\mathcal{R}, \mathbf{I}) \leq \pi\}$ with antipodal surface points identified. Figure 3(b) illustrates that the open ball $\mathcal{B}_\pi(\mathbf{I}_3)$ is diffeomorphic to the open ball $\mathcal{B}_\pi(\mathbf{0}_3)$ which is embedded in Euclidean spaces. Based on the general form of f , the pa-

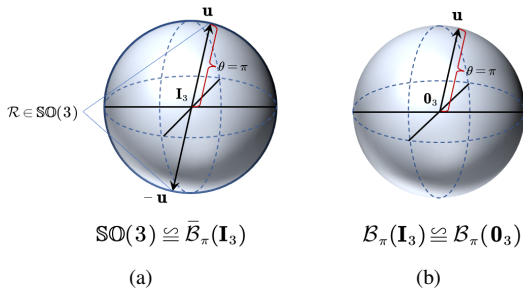


FIG. 3. The geometric configuration of $\mathbb{SO}(3)$ and $\mathcal{B}_\pi(\mathbf{0}_3)$. (a). A solid closed ball $\mathcal{B}_\pi(\mathbf{I}_3)$ with antipodal surface points identified. (b). An open ball $\mathcal{B}_\pi(\mathbf{I}_3)$ diffeomorphic to the open ball $\mathcal{B}_\pi(\mathbf{0}_3)$.

rameterized attitude representations and their corresponding configuration spaces in \mathbb{R}^3 are given in Table II.

E. Rigid body dynamics

There are generally two approaches that describe the dynamics of rigid body systems: Newton-Euler equations and Euler-Lagrange equations.

1. Newton-Euler equation

The Newton-Euler equation is established by Newton's law of motion combining with the Euler equation for the rotational motion as follows,

$$\begin{aligned} m_i \dot{\mathbf{v}}_i &= \mathbf{f}_i, \\ \mathbf{J}_i \dot{\boldsymbol{\omega}}_i &= -\boldsymbol{\omega}_i^\wedge \mathbf{J}_i \boldsymbol{\omega}_i + \boldsymbol{\tau}_i, \end{aligned} \quad (15)$$

where $m_i \in \mathbb{R}$ is the mass, $\mathbf{J}_i \in \mathbb{R}^{3 \times 3}$ the inertia matrix, $\mathbf{v}_i \in \mathbb{R}^3$ the velocity, $\mathbf{f}_i \in \mathbb{R}^3$ the external force, and $\boldsymbol{\tau}_i \in \mathbb{R}^3$ the external torque.

2. Euler-Lagrange equation

The Euler-Lagrange equation of a rigid body system can be formulated as

$$\mathbf{M}_i(\mathbf{q}_i) \ddot{\mathbf{q}}_i + \mathbf{C}_i(\dot{\mathbf{q}}_i, \mathbf{q}_i) \dot{\mathbf{q}}_i + \mathbf{G}_i(\mathbf{q}_i) = \boldsymbol{\Gamma}_i, \quad (16)$$

where $\mathbf{q}_i \in \mathbb{R}^n$ is the generalized coordinate, $\boldsymbol{\Gamma}_i \in \mathbb{R}^n$ the control torque, $\mathbf{M}_i(\mathbf{q}_i) \in \mathbb{R}^{n \times n}$ the inertia matrix, $\mathbf{C}_i(\dot{\mathbf{q}}_i, \mathbf{q}_i) \dot{\mathbf{q}}_i \in \mathbb{R}^n$ the centrifugal/Coriolis force vector, and $\mathbf{G}_i(\mathbf{q}_i) \in \mathbb{R}^n$ the vector of gravitational force.

It should be noted that the Euler-Lagrange system has three important properties as follows:

- P.1: The matrix $\dot{\mathbf{M}}_i(\mathbf{q}_i) - 2\mathbf{C}_i(\dot{\mathbf{q}}_i, \mathbf{q}_i)$ is skew symmetric.
- P.2: The inertia matrix $\mathbf{M}_i(\mathbf{q}_i)$ is a symmetry positive definite matrix, and the norm of Centrifugal/Coriolis matrix satisfies $\|\mathbf{C}_i(\dot{\mathbf{q}}_i, \mathbf{q}_i)\| \leq k_C \|\dot{\mathbf{q}}_i\|$, where k_C is a positive real number. The norm of the gravity vector satisfies $\|\mathbf{G}_i(\mathbf{q}_i)\| \leq k_g$, where k_g is a positive real number.
- P.3: For vectors $\mathbf{x}, \mathbf{y} \in \mathbb{R}^n$, there exists a linear regressor matrix $\mathbf{Y}_i(\dot{\mathbf{q}}_i, \mathbf{q}_i, \mathbf{x}, \mathbf{y})$ satisfying $\mathbf{M}_i(\mathbf{q}_i)\mathbf{x} + \mathbf{C}_i(\dot{\mathbf{q}}_i, \mathbf{q}_i)\mathbf{y} + \mathbf{G}_i(\mathbf{q}_i) = \mathbf{Y}_i(\dot{\mathbf{q}}_i, \mathbf{q}_i, \mathbf{x}, \mathbf{y})\boldsymbol{\Theta}_i$, where $\boldsymbol{\Theta}_i \in \mathbb{R}^m$ is a constant vector representing the real constant parameter of Euler-Lagrange systems.

In fact, the Euler-Lagrange equation is equivalent to Newton-Euler equation. The difference is that the Euler-Lagrange equation is derived based on the principle of the least action, which is a more general and fundamental principle¹⁵. The Newton-Euler equation is based on Newton's laws of motion. It provides a more direct way of calculating the force and torques acting on a rigid body, which is commonly used in a relatively simple motion control design of rigid bodies. Euler-Lagrange equations provide a complete description of the motion of a rigid body. Thus, it is useful in describing a complex dynamic model when the forces and torques are particularly complicated. In addition, it can design the control input of rotational and translational motion in a unified manner⁶⁰.

F. Definitions

Before introducing the main results, we firstly give some basic definitions of attitude synchronization convergence of multiple rigid body systems. Let the consensus set $\mathcal{A} \subseteq \mathbb{SO}(3)^N$ be defined as $\mathcal{A} = \{\mathcal{R} = \{\mathcal{R}_1, \dots, \mathcal{R}_N\} : \mathcal{R}_i = \mathcal{R}_j, \forall i, j = 1, \dots, N\}$. A local attitude synchronization definition is firstly given as follows.

Definition 2¹⁷ Consider a multiple rigid body system that consists of N rigid bodies. Assuming that the initial attitude $\mathcal{R}_i(t_0)$ of each rigid body is contained in a positively invariant set $\mathcal{B}_r(\mathbf{I}_3)$ where $r < \pi$, the local attitude consensus is achieved if $\mathcal{R}(t) \rightarrow \mathcal{A}$ as $t \rightarrow \infty$ for $i = 1, \dots, N, t \geq 0$.

According to the property that the set $\mathbb{SO}(3) - \mathcal{B}_\pi(\mathbf{I}_3)$ has measure zero, we have the following almost global attitude synchronization definition.

Definition 3¹⁷ Consider a multiple rigid body system that consists of N rigid bodies. Assuming that the initial attitude $\mathcal{R}_i(t_0)$ of each rigid body is contained in a positively invariant set $\mathcal{B}_\pi(\mathbf{I}_3)$, the almost global attitude consensus is achieved if $\mathcal{R}(t) \rightarrow \mathcal{A}$ as $t \rightarrow \infty$ for $i = 1, \dots, N, t \geq 0$.

The convergence speed is an important performance in the engineering application of multiple rigid body systems. Next, we give the finite-time, fixed-time, and prescribed-time synchronization definitions, respectively.

Definition 4⁶¹ Consider a multiple rigid body system that consists of N rigid bodies. The finite-time attitude synchronization is locally achieved if the attitude $\mathcal{R}_i(t, \mathcal{R}_i(t_0), t_0), \forall t_0 > 0, \mathcal{R}(t_0) \in \mathcal{B}_r(\mathbf{I}_3), r < \pi$ reaches \mathcal{A} in a settling time $T(\mathcal{R}(t_0), t_0) > 0$, i.e., $\text{dist}(\mathcal{R}(T(\mathcal{R}(t_0), t_0), \mathcal{R}(t_0), t_0), \mathcal{A})) = 0$ and $\text{dist}(\mathcal{R}(t, \mathcal{R}(t_0), t_0), \mathcal{A}) \equiv 0$ for all $t > T(\mathcal{R}(t_0), t_0)$.

Definition 5⁶¹ Consider a multiple rigid body system that consists of N rigid bodies. The fixed-time attitude synchronization is locally achieved if the finite-time attitude synchronization is achieved, and the settling time $T(\mathcal{R}(t_0), t_0)$ is uniformly bounded with the initial value $\mathcal{R}(t_0)$, i.e., $\exists T_{\max} > 0$ such that $T_{\max} \geq T(\mathcal{R}(t_0), t_0), \forall \mathcal{R}(t_0) \in \mathcal{B}_r(\mathbf{I}_3), r < \pi$.

Definition 6 Consider a multiple rigid body system that consists of N rigid bodies. The predefined-time attitude synchronization is locally achieved if the finite-time attitude synchronization is achieved, and the settling time T is predefined such that $T \leq T_{\max}$, where T_{\max} is bounded with initial value $\mathcal{R}(t_0)$, i.e., $\exists T_{\max} > 0$ such that $T_{\max} \geq T(\mathcal{R}(t_0), t_0), \forall \mathcal{R}(t_0) \in \mathcal{B}_r(\mathbf{I}_3), r < \pi$.

Similarly, the almost global finite-time/fixed-time/prescribed-time attitude synchronization are achieved when $r = \pi$ in Definitions 4, 5, and 6 are satisfied.

III. ATTITUDE SYNCHRONIZATION OF MULTIPLE RIGID BODY SYSTEMS

The attitude synchronization literature can be divided into two categories. One is to use parameterized attitude representations. The attitude of each rigid body evolved on \mathbb{R}^3 or \mathbb{S}^3 . The other one is to view the attitude as an element on $\mathbb{SO}(3)$. At last, the recent result on networked attitude synchronization is discussed. A literature summary of this section is shown in Table III.

A. Parameterized attitude synchronization on \mathbb{R}^3

An early work of a cooperative control of multiple rigid bodies by using parameterized attitude synchronizations is considered in the leader-follower framework⁶³. The attitude of rigid bodies is represented by Modified Rodriguez parameters (MRPs). The kinematics of rigid body systems by using MRPs are shown in (11). The control objectives in this work are two aspects. One is that the followers are "dragged" by leaders into the convex hull of the leaders' orientations. The leaders are assumed to converge to the final orientations and the angular velocities will converge to zero, i.e.,

$$\sigma_i = \sigma_i^d, \quad \omega_i = 0, \quad i \in \mathcal{N}^l, \quad (17)$$

where \mathcal{N}^l is the node set of leaders. The other case is to drive the leaders to the desired relative orientations. The relative orientation for each pair of leaders $(i, j) \in \mathcal{E}$ could be different which is given as $\sigma_{ij}^d \in \mathbb{R}^3$. The problem is motivated by the real applications in the multiple satellite scheme. The coordination observation task requires a group of satellite covering a specific area. The leaders' orientations dictate the "boundary" of the area to be covered²².

For the first case, the control law of the followers is given as

$$\tau_i = -\mathbf{G}^\top(\sigma_i) \sum_{j \in \mathcal{N}_i^f} (\sigma_i - \sigma_j) - \sum_{j \in \mathcal{N}_i^f} (\omega_i - \omega_j), \quad i \in \mathcal{N}^f, \quad (18)$$

where \mathcal{N}^f is the node set of followers. For the second case, the control law of the leaders is given as

$$\tau_i = -\mathbf{G}^\top(\sigma_i) \sum_{j \in \mathcal{N}_i^l} (\sigma_i - \sigma_j - \sigma_{ij}^d) - \sum_{j \in \mathcal{N}_i^l} (\omega_i - \omega_j), \quad i \in \mathcal{N}^l \setminus \{\alpha\}, \quad (19)$$

where a leader $\alpha \in \mathcal{N}^l$ is a reference attitude with respect to the desired relative orientation. Here, it is assumed that this leader has already been stabilized to the desired orientation, i.e., $\sigma_\alpha = \sigma_\alpha^d, \quad \omega_\alpha = 0$.

The form of protocols (18), (19) are similar to the second-order consensus protocol for multi-agent systems. However, the difference is that the attitude is governed by the dynamic model (15). Based on the connected topology condition and the properties of the matrix $\mathbf{G}(\sigma_i)$, we can show that the protocol (18) can drive the followers to the convex hull of the leaders' orientations. Furthermore, if no global objective is imposed by the leaders, i.e., $\mathcal{N}^l = \emptyset$. The following proposed distributed attitude synchronization protocol can drive the group of rigid bodies to a common constant orientation with zero angular velocities,

$$\tau_i = -\mathbf{G}^\top(\sigma_i) \sum_{j \in \mathcal{N}_i} (\sigma_i - \sigma_j) - \sum_{j \in \mathcal{N}_i} (\omega_i - \omega_j) - a_i \omega_i, \quad (20)$$

where a_i is the gain of the damp term.

The above protocols require the angular velocity measurement. An angular velocity-free framework motivated by

Attitude representations	Configuration space	Measurement	Convergence	Topology	Communication	Reference
Euler angles	\mathbb{R}^3	Absolute	Local	Fixed	Continuous	16,62
Modified Rodrigues Parameters	\mathbb{R}^3	Absolute	Local	Fixed	Continuous	18,22,63
Axis-angles	\mathbb{R}^3	Absolute	Almost global	Switching	Continuous	28
				Fixed	Event-triggered	17
		Relative	Local	Switching	Continuous	57
				Switching	Event-triggered	64
Quaternions	\mathbb{S}^3	Absolute	Global(Unwinding)	Fixed	Continuous	31,65
				Fixed	Sampled-data	66
				Switching	Continuous	31,65
		Absolute	Global	Fixed	Continuous	23,67
				Fixed	Event-triggered	68,69
Rotation matrices	$\mathbb{SO}(3)$	Absolute	Local	Fixed	Continuous	26,70
		Absolute	Almost global	Fixed	Continuous	24
		Relative	Local	Fixed	Continuous	71
		Relative	Almost global	Fixed	Continuous	29,42,44

TABLE III. A literature summary of coordination control of multiple rigid body systems.

the passivity approach is proposed for multiple rigid body systems²². The control protocol is designed as follows,

$$\dot{\hat{\mathbf{x}}}_i = \mathbf{\Gamma} \hat{\mathbf{x}}_i + \sum_{j=1}^n b_{ij} (\boldsymbol{\sigma}_i - \boldsymbol{\sigma}_j) + \kappa \boldsymbol{\sigma}_i \quad (21)$$

$$\mathbf{y}_i = \mathbf{P} \mathbf{\Gamma} \hat{\mathbf{x}}_i + \mathbf{P} \sum_{j=1}^n b_{ij} (\boldsymbol{\sigma}_i - \boldsymbol{\sigma}_j) + \kappa \mathbf{P} \boldsymbol{\sigma}_i \quad (22)$$

$$\boldsymbol{\tau}_i = -\mathbf{G}^\top (\boldsymbol{\sigma}_i) \left[\sum_{j=1}^n a_{ij} (\boldsymbol{\sigma}_i - \boldsymbol{\sigma}_j) + a_{i(n+1)} (\boldsymbol{\sigma}_i - \boldsymbol{\sigma}_c^r) + \mathbf{y}_i \right], \quad (23)$$

where $\boldsymbol{\sigma}_c^r \in \mathbb{R}^3$ denotes the constant reference attitude for each rigid body, a_{ij} and b_{ij} are entries of two adjacency matrices \mathbf{A} and \mathbf{B} associated with the communication graph, κ is a positive parameter, and $\mathbf{P} = \mathbf{P}^\top \in \mathbb{R}^{3 \times 3}$ is the solution of the Lyapunov equation $\mathbf{\Gamma}^\top \mathbf{P} + \mathbf{P} \mathbf{\Gamma} = -\mathbf{Q}$ with $\mathbf{Q} = \mathbf{Q}^\top > 0 \in \mathbb{R}^{3 \times 3}$. Note that the term $\sum_{j=1}^n b_{ij} (\boldsymbol{\sigma}_i - \boldsymbol{\sigma}_j)$ in (21) provides the relative damping between neighboring rigid bodies, and the output signal \mathbf{y}_i replaces the angular velocity feedback in the control torque.

Note that MRPs describe the attitude as a vector in Euclidean spaces, which makes the synchronization protocol design and convergence analysis convenient. There are other results of attitude synchronization based on MRPs⁷². Motivated by the precise requirement of completing time in some aerospace tasks, finite-time attitude synchronization has been widely studied¹⁸. A distributed finite-time attitude containment control is studied for multiple rigid body systems¹⁸. The multiple stationary leaders and dynamic leaders are both considered. Two kinds of distributed protocols are designed to guarantee that followers' attitudes converge to the convex hull formed by leaders in finite time. However, the estimation settling time of the finite-time consensus protocol is quite conservative. In addition, it depends on the initial attitude and parameters of rigid bodies. A prescribed-time attitude consensus problem is studied using MRPs where the users can predetermine the settling time⁷³. However, the parameterized

attitude representation on \mathbb{R}^3 has a singularity problem. For MRPs, the singularity point corresponds to the attitude that the rotation angle approaches 2π ²².

B. Parameterized attitude synchronization on \mathbb{S}^3

The unit quaternion is a global attitude representation²¹. A coordinated attitude control problem for multiple rigid body systems is investigated with communication delays and without angular velocity measurements based on unit quaternions⁷⁴. This work proposed a virtual dynamic system approach to handle the communication delay and remove the requirement of angular velocity measurements. The first virtual system associates to each rigid body is formulated as

$$\dot{\mathbf{Q}}_{v_i} = \frac{1}{2} \mathbf{T}(\mathbf{Q}_{v_i}) \boldsymbol{\omega}_{v_i} \quad (24)$$

for $i \in \mathcal{N}$, where $\mathbf{Q}_{v_i} = (\mathbf{q}_{v_i}^\top, \eta_{v_i})^\top$ is the unit quaternion representing the state of the virtual system (24). The $\mathbf{Q}_{v_i}(0)$ can be initialized arbitrarily, and $\boldsymbol{\omega}_{v_i}$ is the virtual angular velocity input which will be designed later. The matrix $\mathbf{T}(\mathbf{Q}_{v_i})$ is

$$\mathbf{T}(\mathbf{Q}_{v_i}) = \begin{pmatrix} \eta_{v_i} \mathbf{I}_3 + \mathbf{S}(\mathbf{q}_{v_i}) \\ -\mathbf{q}_{v_i}^\top \end{pmatrix}.$$

The second virtual system is formulated as

$$\dot{\mathbf{P}}_i = \frac{1}{2} \mathbf{T}(\mathbf{P}_i) \boldsymbol{\beta}_i, \quad (25)$$

where \mathbf{P}_i is the unit quaternion representing the state of the virtual system (25), and the initial values can be given arbitrarily. $\mathbf{T}(\mathbf{P}_i)$ is given similar to (24), and $\boldsymbol{\beta}_i \in \mathbb{R}^3$ is an input to be determined.

The main idea in this approach is to design the control input $\boldsymbol{\tau}_i$ for each rigid body as well as the input for virtual systems associated with each rigid body. The control input $\boldsymbol{\tau}_i$ is designed based on the signal constructed by the state of these two virtual systems without requiring the angular velocity measurement. The control input for each rigid body system

is designed as

$$\boldsymbol{\tau}_i = \mathbf{H}_i(\dot{\boldsymbol{\omega}}_{v_i}, \boldsymbol{\omega}_{v_i}, \mathbf{Q}_i^e) - k_i^p \mathbf{q}_i^e - k_i^d \tilde{\mathbf{q}}_i^e, \quad i \in \mathcal{N}, \quad (26)$$

where

$$\mathbf{H}_i(\dot{\boldsymbol{\omega}}_{v_i}, \boldsymbol{\omega}_{v_i}, \mathbf{Q}_i^e) = \mathbf{I}_f \mathbf{R}(\mathbf{Q}_i^e) \dot{\boldsymbol{\omega}}_{v_i} + (\mathbf{R}(\mathbf{Q}_i^e) \boldsymbol{\omega}_{v_i})^\wedge \mathbf{I}_f \mathbf{R}(\mathbf{Q}_i^e) \boldsymbol{\omega}_{v_i}, \quad (27)$$

and k_i^p, k_i^d are strictly positive scalar gains, \mathbf{q}_i^e is the vector part of the unit quaternion $\mathbf{Q}_i^e = (\mathbf{q}_i^{e\top}, \eta_i^e)^\top$ which is defined as $\mathbf{Q}_i^e = \mathbf{Q}_{v_i}^{-1} \odot \mathbf{Q}_i$, and $\tilde{\mathbf{q}}_i^e$ is the vector part of the unit quaternion $\tilde{\mathbf{Q}}_i^e = (\tilde{\mathbf{q}}_i^{e\top}, \tilde{\eta}_i^e)^\top$ which is defined as $\tilde{\mathbf{Q}}_i^e = \mathbf{P}_i^{-1} \odot \mathbf{Q}_i^e$. The control inputs for two virtual systems are given as

$$\dot{\boldsymbol{\omega}}_{v_i} = -k_i^\omega \boldsymbol{\omega}_{v_i} - \sum_{j=1}^n k_{ij} \bar{\mathbf{q}}_{v_{ij}}, \quad (28)$$

and

$$\beta_i = \lambda_i \tilde{\mathbf{q}}_i^e, \quad i \in \mathcal{N}, \quad (29)$$

where $\boldsymbol{\omega}_{v_i}(0)$ can be selected arbitrarily, $\bar{\mathbf{q}}_{v_{ij}}$ is the vector part of the unit quaternion $\bar{\mathbf{Q}}_{v_{ij}} = \mathbf{Q}_{v_j}^{-1}(t - \tau_{ij}) \odot \mathbf{Q}_{v_i}$. The scalar gains $k_i^q > 0, k_i^\omega > 0, \lambda_i > 0$ for $i \in \mathcal{N}$, and $k_{ij} \geq 0$ is the $(i, j)^{th}$ entry of the adjacency matrix of the weighted undirected graph \mathcal{G} . Based on the control input (26)-(29), if the control gain satisfies $k_i^p - \sum_{j=1}^N (\frac{k_{ij}}{4})(\varepsilon + (\frac{\tau^2}{\varepsilon})) > 0$ where τ is the upper bound of the time-varying communication delays such that $\tau_{ij} \leq \tau$ for $(i, j) \in \mathcal{E}$, the attitude synchronization can be attained.

The difference between the angular velocity-free approach (26) and (23) lie in the dynamics of attitude. The attitude configuration space is Euclidean space in (21). However, in (24), the virtual state is governed by the unit quaternion dynamics, which is nonlinear. The benefit of the approach in (26) is that it can be used in the relative attitude measurement case, and the unit quaternion can describe attitude globally without singularity problems. Numerous results on attitude synchronization based on unit quaternions have been made. An angular velocity-free leader-follower attitude consensus with a dynamic leader is solved by proposing a distributed unit quaternion-based attitude feedback control law⁵⁹. A distributed observer is proposed to estimate the leader's state, and an auxiliary system is designed to compensate for the angular velocity. Following this distributed observer approach, the leader-following attitude consensus that is subject to jointly connected switching topologies⁶⁵ and sampled-data scheme⁶⁶ are studied by using unit-quaternion representations.

Although the unit quaternion can describe attitudes globally, it is a non-unique representation. The non-unique attitude representation can lead to an undesirable phenomenon called unwinding. In unwinding, for certain initial conditions under attitude kinematic (14), the trajectories can undergo a homoclinic-like orbit that starts close to the desired attitude equilibrium¹⁹. Thus, the quaternion-based attitude synchronization scheme may achieve global synchronization. However, the synchronization state can be stable or unstable²³.

Motivated by this fact, a hybrid feedback using unit quaternions that achieves the global attitude synchronization is proposed for each rigid body²³. The unwinding phenomenon can be avoided by using a logic variable associated with each pair of rigid bodies which determines the sign of a torque input component.

Let $h = \{h_1, h_2, \dots, h_M\} \in \{-1, 1\}^M$ denote a binary logic variable vector, where h_k is associated with each link $k \in \mathcal{M}$ in the graph. Let the flow set C_i and jump set D_i for rigid body i be given as

$$C_i = \{x \in \mathcal{X} : \forall k \in \mathcal{M}_i^+, h_k \tilde{\eta}_k \geq -\delta\} \quad (30)$$

$$D_i = \{x \in \mathcal{X} : \exists k \in \mathcal{M}_i^+, h_k \tilde{\eta}_k \leq -\delta\}, \quad (31)$$

where δ is a positive constant, \mathcal{X} is the state space, and $\tilde{\eta}_k$ is the scalar component of the relative attitude error for each link $k \in \mathcal{M}$. The hybrid dynamics of the binary logic variable h_k is given as

$$\forall k \in \mathcal{M}_i^+ \quad \begin{cases} \dot{h}_k = 0 & x \in C_i \\ h_k^+ \in h_k \overline{\text{sgn}}(h_k \tilde{\eta}_k + \alpha) & x \in D_i, \end{cases} \quad (32)$$

where $\alpha \in [0, \delta)$, and the set-valued map $\overline{\text{sgn}} : \mathbb{R} \rightrightarrows \{-1, 1\}$ is defined as

$$\overline{\text{sgn}}(s) = \begin{cases} s/|s| & s \neq 0 \\ \{-1, 1\} & s = 0. \end{cases}$$

Based on the logic variable and the reference angular velocity signal $\boldsymbol{\omega}_d$, the control torque is given as,

$$\boldsymbol{\tau}_i = -(\mathbf{J}_i \boldsymbol{\omega}_i)^\wedge \boldsymbol{\omega}_d - \sum_{k=1}^M b_{ik} h_k \ell_k \tilde{\boldsymbol{\epsilon}}_k - K_i \bar{\boldsymbol{\omega}}_i, \quad (33)$$

where $l_k > 0, \forall k \in M, \bar{\boldsymbol{\omega}}_i = \boldsymbol{\omega}_i - \boldsymbol{\omega}_d$, and $K_i = K_i^\top > 0, \forall i \in \mathcal{N}$.

The binary logic variable incorporated in the control law (33) can hysterically switch the sign of a torque component which has an anti-unwinding property. In addition, the hybrid control law (33) can achieve the robust attitude synchronization under the connected acyclic graphs, and manage a trade-off between unwinding and robustness by adjusting the hysteresis width δ . Based on the hybrid control, there are fruitful results on global attitude synchronization⁶⁹. For example, the global finite-time attitude consensus is investigated with quaternion-based hybrid controllers⁶⁷. A hybrid attitude tracking control is studied based on the event-triggered mechanism⁷⁵.

The rotation matrix is a global and unique attitude representation method. However, the closed-loop dynamics by using a continuous state-feedback based on rotation matrices usually has undesired equilibrium points which are unstable. The fundamental difficulty is the underlying space of rotation matrices is a Lie group, which is not homeomorphic to \mathbb{R}^n . Inspired by the above hybrid method²³, a hybrid-based attitude tracking controller on $\mathbb{S}\mathbb{O}(3)$ is proposed to obtain the global result⁷⁶. Following the idea, an angular velocity-free global attitude tracking on $\mathbb{S}\mathbb{O}(3)$ and $\mathbb{S}\mathbb{E}(3)$ are further studied, respectively^{77,78}.

C. Attitude synchronization on $\mathbb{SO}(3)$

Due to the topological complexities of $\mathbb{SO}(3)$, there is no smooth state-feedback control that can globally solve the attitude stabilization. Thus, the best result of using the smooth control protocol is almost global attitude synchronization²⁹. The attitude synchronization is considered with switching topologies for multiple rigid body systems²⁸. The rotation of each rigid body is described by the axis-angle representation which can almost globally represent the attitude. The axis-angle representation of the absolute attitude measurement and the relative attitude measurement can be calculated by using the logarithm map

$$\mathbf{x}_i^\wedge = \log(\mathcal{R}_i), \quad (34)$$

and

$$\mathbf{x}_{ij}^\wedge = \log(\mathcal{R}_i^\top \mathcal{R}_j), \quad (35)$$

where $\mathbf{x}_i^\wedge \in \mathfrak{so}(3)$ is the skew-symmetric matrix generated by $\mathbf{x}_i = [x_i^1, x_i^2, x_i^3] \in \mathbb{R}^3$. Based on the absolute attitude measurement and the relative attitude measurement information, the attitude synchronization protocols are given as follows,

$$\omega_i^a = \sum_{j \in \mathcal{N}_i(t)} a_{ij}(t)(\mathbf{x}_j - \mathbf{x}_i), \quad (36)$$

and

$$\omega_i^r = \sum_{j \in \mathcal{N}_i(t)} a_{ij}(t)(\mathbf{x}_{ij}), \quad (37)$$

where $a_{ij}(t)$ is a weighted matrix associated with the time-varying graph $\mathcal{G}(t)$ in Definition 1, ω_i^a and ω_i^r are the angular velocity inputs based on absolute attitude measurements and relative attitude measurements for rigid body i , respectively.

It can be proven that the first protocol (36) guarantees the positive invariance of the open ball $\mathcal{B}_\pi(\mathbf{0})$ which can almost globally cover $\mathbb{SO}(3)$. Thus, the almost global attitude synchronization is achieved by using (36). For the relative attitude measurement only case, the convergence result is based on the convex property on the local set $\mathcal{B}_{\frac{\pi}{2}}(\mathcal{Q})$, where \mathcal{Q} is an arbitrary rotation on $\mathbb{SO}(3)$. In addition, the protocol input (37) can be interpreted from the geometric view, which is inward-pointing to the boundary of the convex hull on $\mathcal{B}_{\frac{\pi}{2}}(\mathcal{Q})$. It can be shown that the convex hull is shrinking and further shrinks to one point, which achieves the local attitude synchronization⁷⁹. The above results²⁸ are quite interesting since it only uses the well-known consensus protocol as shown in (36) to achieve the attitude synchronization, which allows methods that are suitable to the Euclidean space \mathbb{R}^3 . The local and almost global finite-time attitude consensus in Definition 4 are achieved based on a discontinuous attitude consensus protocol⁸⁰. However, the discontinuous control input signal may not be appropriate for the implementation in the mechanical system, which is harmful to the actuator. A fixed-time attitude consensus protocol is designed by constructing a class of particularly continuous functions⁶¹.

Different from the complete attitude synchronization on $\mathbb{SO}(3)$, a reduced attitude can be considered as an element on two-dimensional spheres¹⁹. Incomplete attitude synchronization corresponds to practical problems such as moving along a common direction in flocks and pointing to a common direction in a network of satellites. A common framework of synchronization of agents on \mathbb{S}^2 and $\mathbb{SO}(3)$ is proposed under switching topologies³¹. The complete attitude synchronization is cast as synchronization on \mathbb{S}^3 and the incomplete attitude synchronization is cast as synchronization on \mathbb{S}^2 . It should be noted that the consensus problem on \mathbb{S}^n has a strong application background, including reduced attitude synchronization³¹, self-synchronizing oscillators^{81–83}, and quantum consensus^{38,39}. The almost global consensus result is established for a class of consensus protocols on n -spheres except for the circle in²⁹. The agent's state $\mathbf{x}_i \in \mathbb{S}^n$ and dynamics is governed by

$$\dot{\mathbf{x}}_i = \mathbf{u}_i - \langle \mathbf{u}_i, \mathbf{x}_i \rangle \mathbf{x}_i = (\mathbf{I} - \mathbf{X}_i) \mathbf{u}_i = \mathbf{P}_i \mathbf{u}_i, \quad (38)$$

where $\mathbf{u}_i : \mathcal{I}_i \rightarrow \mathbb{R}^{n+1}$ is the input signal of agent i , $\mathbf{X}_i = \mathbf{x}_i \otimes \mathbf{x}_i$, and $\mathbf{P}_i = \mathbf{I} - \mathbf{X}_i$ for all $i \in \mathcal{V}$. The dynamics of the state $\mathbf{x}_i \in \mathbb{S}^n$ (38) can be derived from the dynamics on $\mathbb{SO}(n)$. In fact, the state $\mathbf{x}_i \in \mathbb{S}^n$ can be seen as a column of the matrix $\mathcal{R}_i \in \mathbb{SO}(n)$. From this point of view, letting $\mathcal{R}_i[1, 0, \dots, 0]^\top = \mathbf{x}_i$, the dynamics of \mathbf{x}_i can be written as $\dot{\mathbf{x}} = \mathbf{P}_i \mathbf{u}_i$, where \mathbf{P}_i is a projector that transforms the input \mathbf{u}_i onto the tangent space at the point \mathbf{x}_i ⁴³.

The consensus algorithm is derived by taking the gradient of the following Lyapunov function $V : (\mathbb{S}^n)^N \rightarrow [0, +\infty)$,

$$V \left((\mathbf{x}_i)_{i=1}^N \right) = \sum_{\{i,j\} \in \mathcal{E}} \int_0^{s_{ij}} f_{ij}(r) dr, \quad (39)$$

where $s_{ij} = 1 - \langle \mathbf{x}_i, \mathbf{x}_j \rangle$ and $f_{ij} : \mathbb{R} \rightarrow \mathbb{R}$ is a real analytic function satisfying the following condition: i) $f_{ij} > 0$; ii) $f_{ij} = f_{ji}$; and iii) $(n-2+s_{ij})s_{ij}f_{ij} - (2-s_{ij})s_{ij}^2 f'_{ij} > 0$ for all $s_{ij} \in (0, 2]$ and all $\{i, j\} \in \mathcal{E}$. By embedding the sphere \mathbb{S}^n in \mathbb{R}^{n+1} , the extension function $U : (\mathbb{R}^{n+1})^N \rightarrow \mathbb{R}$ can be given by

$$U \left((\mathbf{x}_i)_{i=1}^N \right) = \sum_{\{i,j\} \in \mathcal{E}} \int_0^{s_{ij}} f_{ij}(r) dr. \quad (40)$$

Then, the control protocol can be obtained by

$$\mathbf{u}_i = -\nabla_i U = - \sum_{j \in \mathcal{N}_i} \frac{dU}{ds_{ij}} \nabla_i s_{ij} = \sum_{j \in \mathcal{N}_i} f_{ij}(s_{ij}) \mathbf{x}_j, \quad (41)$$

where ∇_i denotes $\nabla_{\mathbf{x}_i}$.

It can be shown that when the protocol (41) is utilized, the almost global consensus on n -sphere, $n \in \mathbb{N} \setminus \{1\}$ is reached. To show this result, the first step is to prove that the consensus set \mathcal{C} is asymptotically stable. This fact can be obtained since the right hand side of (38) points toward the geodesically convex hull of $\{\mathbf{x}_j | j \in \mathcal{N}_i\}$ on \mathbb{S}^n . The second step is to prove the instability of the undesired equilibrium points on \mathbb{S}^n . This fact is derived by using the linearized around the equilibrium

points and due to the property of the gain function f_{ij} . Then, combining these facts, the almost global consensus results can be obtained. This analysis procedure is also suitable for consensus problems on more general manifolds.

The attitude of rigid bodies is an element in the special orthogonal group, i.e., $\mathbb{SO}(3)$. More generally, it can be considered as a smooth manifold. A distributed consensus algorithm with the states lying in a Riemannian manifold is proposed for a multi-agent system⁷¹. The idea of the algorithm is to formulate the consensus problem as an optimization problem and define the cost function on Riemannian manifold, which describes the disagreement of distances for multi-agent systems. The cost function on Riemannian manifold is given as

$$\varphi(\mathbf{x}) = \frac{1}{2} \sum_{\{i,j\} \in E} d^2(\mathbf{x}_i, \mathbf{x}_j), \quad (42)$$

where $\mathbf{x}_i \in \mathcal{M}$, \mathcal{M} denotes a Riemannian manifold, and $d(\mathbf{x}_i, \mathbf{x}_j)$ is the geodesic distance between \mathbf{x}_i and \mathbf{x}_j . The distributed algorithm of each node is obtained through Riemannian gradient descent. The update rule of each agent is obtained by calculating the gradient of φ with respect to \mathbf{x}_i as follows,

$$\text{grad}_{\mathbf{x}_i} \varphi = \frac{1}{2} \text{grad}_{\mathbf{x}_i} \sum_{j \in \mathcal{N}_i} d^2(\mathbf{x}_i, \mathbf{x}_j) = - \sum_{j \in \mathcal{N}_i} \log_{\mathbf{x}_i}(\mathbf{x}_j), \quad (43)$$

where \log is the logarithm map. The main result discusses relationships between the convergence of the algorithm and domain of attraction on Riemannian manifold as well as topology graphs. Based on (43), if the initial states are contained in the set $\mathcal{S}_{conv} = \{\mathbf{x} \in \mathcal{M}^N : \varphi(\mathbf{x}) < \frac{(r^*)^2}{2D}\}$, where D is the diameter of the graph \mathcal{G} and r^* is the convexity radius of the manifold, the consensus can be achieved if step size $\varepsilon \in (0, 2\mu_{\max}^{-1})$ is admissible. The upper bound of the parameter μ_{\max} for the step size is determined according to the curvature of the manifold.

The above consensus result requires undirected graphs and the convexity property for the manifold in the convergence analysis. To relax the requirement, a novel control scheme for synchronization on $\mathbb{SO}(d)$ is proposed in a distributed manner⁴⁴. Based on a QR-factorization approach, a dynamic feedback control algorithm is proposed for synchronization of the k first columns of the matrix on $\mathbb{SO}(d)$. Based on the control scheme, the almost global convergence is achieved under strongly connected graphs. A more general result of synchronization on Stiefel manifolds is shown based on the high-dimensional Kuramoto model which covers the case of \mathbb{S}^n and $\mathbb{SO}(n)$ ⁸⁴. Inspired by the above approach²⁹, it is proven that the almost global synchronization of the generalized Kuramoto model on Stiefel manifold $St(p, n)$ is achieved for any connected graphs if the condition $p \leq \frac{2}{3}n - 1$ is satisfied⁸⁴. Furthermore, synchronization on Riemannian manifolds is considered in the sense of geodesic distances and chordal distances for manifolds, respectively⁴¹. It is shown that, if the manifold is multiply connected or contains a closed geodesic that is of locally minimum length in a space of closed curves, the consensus algorithms are multi-stable. Note that the previous result on \mathbb{S}^n and $\mathbb{SO}(n)$ is a special case of this result⁴¹.

D. Sampled-data based attitude synchronization

In general, attitude synchronization is realized by means of information sharing through multiple rigid body networks. The data in communication networks is transmitted in the form of digital signals based on sampled-data mechanism rather than continuous signals⁶⁶. In addition, due to the limited bandwidth, network traffic congestion is unavoidable leading to network-induced delays⁷⁴. Recently, attitude synchronization under networked constraints has been studied in different aspects such as communication time delays⁸⁵, sampled-data mechanism⁶⁶, and event-triggered mechanism¹⁷. A leader-following consensus of multiple rigid body systems is studied under a sampled-data communication setting⁶⁶. The dynamics of the leader system is governed by the following system

$$\dot{v} = Sv, \quad \Omega_0 = Ev \quad (44)$$

$$\dot{q}_0 = \frac{1}{2} q_0 \odot \begin{bmatrix} 0 \\ \Omega_0 \end{bmatrix}, \quad (45)$$

where $S \in \mathbb{R}^{m \times m}$ and $E \in \mathbb{R}^{3 \times m}$ are constant matrices with the pair (E, S) detectable, $v \in \mathbb{R}^m$, $\Omega_0 \in \mathbb{R}^3$, and $q_0 = \text{col}(\bar{q}_0, \hat{q}_0) \in \mathbb{S}^3$, $\hat{q}_0 \in \mathbb{R}^3$, $\bar{q}_0 \in \mathbb{R}$.

A sampled-data distributed observer is proposed to estimate the state of the leader system as follows, when $t \in [t_s, t_{s+1})$,

$$\dot{\xi}_i(t) = S\xi_i(t) + L \sum_{j=0}^N a_{ij} E (\xi_j(t_s) - \xi_i(t_s)), \quad (46)$$

$$\dot{\eta}_i(t) = \frac{1}{2} \eta_i(t) \odot \mathbf{Q}(\zeta_i(t)) + \mu \sum_{j=0}^N a_{ij} (\eta_j(t_s) - \eta_i(t_s)), \quad (47)$$

where $L \in \mathbb{R}^{m \times 3}$ is a positive definite matrix, μ is a positive number, $\xi_0 = v$, $\eta_0 = q_0$, and $\zeta_i = E\xi_i$. $t_{s+1} = t_s + T_s$, $s \in \mathbb{N}$ are the sampling instants, and $T_s \in [\underline{h}, \bar{h}]$. One of the main results is to determine the explicit upper bound for the sampling intervals to guarantee the validity of the sampled-data distributed observer.

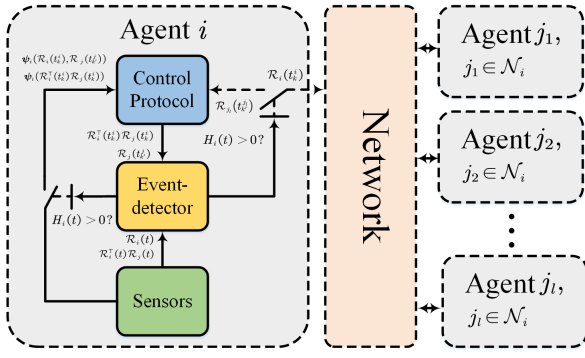
Motivated by the limited communication resource in aerospace applications such as nano-satellite swarms, the continuous attitude synchronization protocol is not feasible. The event-triggered distributed control is widely investigated in the multi-agent systems⁸⁶⁻⁹² as well as rigid body systems^{72,93}. An event-triggered attitude consensus is considered in the absolute attitude measurement and the relative attitude measurement cases¹⁷, respectively. The event-triggered attitude consensus framework is shown in Fig. 4¹⁷. In the first case, a gnomonic mapping is utilized to project the unit-quaternion on a hemi-sphere contained on \mathbb{S}^3 to the Euclidean plane almost globally. Based on the projection $\mathbf{y}_i = \tan \frac{\theta_i}{2} \mathbf{u}_i$, the protocol is designed as

$$\mathbf{w}_i(t) = \sum_{j=1}^N a_{ij} \left(\mathbf{y}_j(t_{k'}^j) - \mathbf{y}_i(t_k^i) \right), \quad t \in [t_k^i, t_{k+1}^i), \quad (48)$$

where $\mathbf{y}_i(t_k^i)$ denotes the i th rigid body's attitude at the triggering instant t_k^i . Let the event-triggered sampling error be

Reference	Graph		Model uncertainty		Velocity-free	Communication			Switching topology
	Undirected	Directed	Parameter linearity	Unmodeled dynamics		Continuous	Sampled-data	Event-triggered	
18,46	✓		✓			✓			
47,50,94,95		✓	✓			✓			
45	✓			✓		✓			
55		✓		✓		✓			
51,96		✓	✓				✓		
53,54,97		✓	✓					✓	
98,99		✓		✓				✓	
100	✓		✓		✓			✓	
101		✓	✓			✓		✓	
102		✓	✓		✓	✓		✓	
103	✓		✓					✓	
104		✓	✓					✓	

TABLE IV. A literature summary of coordination control of multiple rigid body systems.

FIG. 4. The control diagram of event-triggered attitude synchronization¹⁷.

defined as $\mathbf{e}_i(t) = \mathbf{y}_i(t_k^i) - \mathbf{y}_i(t)$, the triggering instant is determined by the following condition

$$t_{k+1}^i = \min_{t \geq t_k^i} \{t \in \mathbb{R} : \|\mathbf{e}_i(t)\| > \alpha_i \|\mathbf{z}_i(t)\|, i = 1, \dots, N\},$$

where $\mathbf{z}_i(t) = \sum_{j=1}^N a_{ij} (\mathbf{y}_j(t_{k'}^j) - \mathbf{y}_i(t_k^i))$, $t \in [t_k^i, t_{k+1}^i)$ and $\alpha_i < \frac{1}{2a_i |\mathcal{A}_i^i|}$. Note that the event-triggered protocol (48) can achieve the almost global attitude consensus due to the property that the configuration space of the projection $\mathbf{y}_i \in \mathcal{B}_r(\mathbf{0})$, where $r = \infty$.

In the second protocol, a gradient vector for a disagreement function using the geodesic distance on $\mathbb{S}\mathbb{O}(3)$ is utilized to achieve attitude synchronization. Define a geodesic distance function as follows

$$\phi = \sum_{i=1}^N \phi_i = \frac{1}{2} \sum_{i=1}^N \sum_{j=1}^N a_{ij} d^2(\mathcal{R}_i, \mathcal{R}_j). \quad (49)$$

Then, the gradient vector of the function ϕ_i at the point \mathcal{R}_i can be calculated by $\nabla_{\mathcal{R}_i} \phi_i := -\sum_{j=1}^N a_{ij} \log(\mathcal{R}_i^\top \mathcal{R}_j)$. Based on

the gradient vector, the protocol is formulated as

$$\begin{aligned} \mathbf{w}_i^\wedge(t) &= -\nabla_{\mathcal{R}_i} \phi_i(t_k^i) \\ &= \sum_{j=1}^N a_{ij} \log(\mathcal{R}_i^\top \mathcal{R}_j)(t_k^i), t \in [t_k^i, t_{k+1}^i). \end{aligned} \quad (50)$$

The event-triggered sampling error is designed on the tangent space of $\mathbb{S}\mathbb{O}(3)$,

$$\begin{aligned} E_i(t) &= \nabla_{\mathcal{R}_i} \phi_i(t) - \nabla_{\mathcal{R}_i} \phi_i(t_k^i) \\ &= \sum_{j=1}^N a_{ij} \log(\mathcal{R}_i^\top \mathcal{R}_j)(t_k^i) - \sum_{j=1}^N a_{ij} \log(\mathcal{R}_i^\top \mathcal{R}_j)(t), \\ & t \in [t_k^i, t_{k+1}^i), \end{aligned} \quad (51)$$

and a dynamic event-triggered condition is given as

$$\begin{aligned} t_{k+1}^i &= \min_{t \geq t_k^i} \left\{ t \in \mathbb{R} : \eta_i(t) + \theta_i \left(\alpha_i \|\nabla_{\mathcal{R}_i}^\vee \phi_i(t)\|^2 \right. \right. \\ & \quad \left. \left. - \|E_i^\vee(t)\|^2 \right) \leq 0, t \in [t_k^i, t_{k+1}^i) \right\}, \end{aligned} \quad (52)$$

where $\theta_i \in \left[\frac{1-\beta_i}{\lambda_i}, +\infty \right)$, and η_i is a dynamic variable inspired by¹⁰⁵. The dynamics are designed as

$$\dot{\eta}_i(t) = -\lambda_i \eta_i(t) + \beta_i \left(\alpha_i \|\nabla_{\mathcal{R}_i}^\vee \phi_i(t)\|^2 - \|E_i^\vee(t)\|^2 \right), \quad (53)$$

where $\eta_i(0) > 0$, $\lambda_i > 0$, $\beta_i \in [0, \frac{1}{2}]$ and $\alpha_i \in [0, 1]$ are non-negative parameters. The proposed event-triggered scheme guarantees the positive invariance of the set $\mathcal{B}_{\frac{\pi}{2}}(\mathcal{Q})$ on $\mathbb{S}\mathbb{O}(3)$, where $\mathcal{Q} \in \mathbb{S}\mathbb{O}(3)$ is a rotation, and the attitude consensus can be achieved by using only relative attitude measurements. The further result, which considers the dynamic model of the rigid body, and the angular velocity-free attitude synchronization scheme is proposed under event-triggered mechanisms⁶⁴.

IV. COORDINATION CONTROL OF MULTIPLE RIGID BODY SYSTEMS

The motion of rigid bodies has total six degree of freedom, i.e., three for orientations and three for positions. It is worth noting that the orientation and the position are often coupled in practical applications of rigid bodies such as formation flying of quadrotors^{70,106}. Different from attitude synchronization which only focuses on the orientation control, the coordination control of multiple rigid body systems pays attention to the position and the orientation control coupled together. A literature summary of this section is shown in Table IV.

A. Coordination control of Euler-Lagrange systems

The Euler-Lagrange equation is an effective method to model the dynamic of mechanical systems in terms of the energy conservation¹⁵. In addition, it allows a unified design of rotation and translation control law coupled together^{10,107}. A distributed leaderless consensus problem is considered for networked Euler-Lagrange systems⁴⁶. The fundamental consensus algorithm is first proposed under the undirected graph. Then, two consensus algorithms accounting of actuator saturation and unavailability of measurements for generalized coordinate derivatives are proposed. However, the undirected graph condition is needed. A distributed containment control problem is considered for networked Euler-Lagrange systems under directed graphs⁹⁵. A distributed sliding mode estimator is given by

$$\begin{aligned}\hat{\mathbf{q}}_{ri} &\triangleq \hat{\mathbf{v}}_i - \alpha \sum_{j \in \mathcal{V}_L \cup \mathcal{V}_F} a_{ij} (\mathbf{q}_i - \mathbf{q}_j), \\ \hat{\mathbf{q}}_{ri} &\triangleq \hat{\mathbf{a}}_i - \alpha \sum_{j \in \mathcal{V}_L \cup \mathcal{V}_F} a_{ij} (\dot{\mathbf{q}}_i - \dot{\mathbf{q}}_j), \\ \hat{\mathbf{s}}_i &\triangleq \dot{\mathbf{q}}_i - \hat{\mathbf{q}}_{ri} = \dot{\mathbf{q}}_i - \hat{\mathbf{v}}_i + \alpha \sum_{j \in \mathcal{V}_L \cup \mathcal{V}_F} a_{ij} (\mathbf{q}_i - \mathbf{q}_j), \quad i \in \mathcal{V}_F,\end{aligned}\quad (54)$$

where \mathbf{q}_i and $\dot{\mathbf{q}}_i$ denote the vector of generalized coordinates and the vector of the derivative of generalized coordinates, respectively. $\hat{\mathbf{v}}_i$ and $\hat{\mathbf{a}}_i$ denote the estimation of the leader's velocity and acceleration, and α is a positive constant. Based on the design of the reference signal and sliding mode variable in (54), the adaptive distributed control protocol can be given by

$$\tau_i = -K_i \hat{\mathbf{s}}_i + Y_i (\mathbf{q}_i, \dot{\mathbf{q}}_i, \hat{\mathbf{q}}_{ri}, \hat{\mathbf{q}}_{ri}) \hat{\Theta}_i, \quad (55)$$

$$\dot{\hat{\mathbf{v}}}_i = -\beta_1 \operatorname{sgn} \left[\sum_{j \in \mathcal{V}_F} a_{ij} (\hat{\mathbf{v}}_i - \hat{\mathbf{v}}_j) + \sum_{j \in \mathcal{V}_L} a_{ij} (\hat{\mathbf{v}}_i - \dot{\mathbf{q}}_j) \right], \quad (56)$$

$$\dot{\hat{\mathbf{a}}}_i = -\beta_2 \operatorname{sgn} \left[\sum_{j \in \mathcal{V}_F} a_{ij} (\hat{\mathbf{a}}_i - \hat{\mathbf{a}}_j) + \sum_{j \in \mathcal{V}_L} a_{ij} (\hat{\mathbf{a}}_i - \ddot{\mathbf{q}}_j) \right], \quad (57)$$

$$\dot{\hat{\Theta}}_i = -\Lambda_i Y_i^\top (\mathbf{q}_i, \dot{\mathbf{q}}_i, \hat{\mathbf{q}}_{ri}, \hat{\mathbf{q}}_{ri}) \hat{\mathbf{s}}_i, \quad i \in \mathcal{V}_F, \quad (58)$$

where $\hat{\Theta}_i$ is the estimation of constant physical parameter Θ_i , $Y_i (\mathbf{q}_i, \dot{\mathbf{q}}_i, \hat{\mathbf{q}}_{ri}, \hat{\mathbf{q}}_{ri})$ is the regression vector, K_i and Λ_i are sym-

metric positive-definite matrices, β_1 and β_2 are positive constants. The estimators (56) and (57) are distributed finite-time observers, which provide the leader's velocity and acceleration estimation for each follower. The adaptive law (58) is designed based on the linear property of Euler-Lagrange models to deal with the unknown physical parameters for rigid bodies. Note that this framework can also solve the leader-follower and leaderless consensus problem for networked Euler-Lagrange systems.

Following this work, there are number of results on coordination control of networked Euler-Lagrange systems^{47,48,108}. A leader-follower flocking algorithm is proposed for the leader with constant velocities and time-varying velocities, respectively, to maintain a connectivity and avoid collisions¹⁰⁹. The key idea of dealing with the collision avoidance and connectivity maintenance is to introduce the potential function V_{ij} as follows: 1) If $\|\mathbf{q}_i(0) - \mathbf{q}_j(0)\| \geq R$, where R is sensing radius of the agents. V_{ij} is a differentiable nonnegative function of $\|\mathbf{q}_i - \mathbf{q}_j\|$ satisfying the conditions: (i) $V_{ij} = V_{ji}$ achieves its unique minimum when $\|\mathbf{q}_i - \mathbf{q}_j\|$ is equal to the value \bar{d}_{ij} , where $\bar{d}_{ij} < R$. (ii) $V_{ij} \rightarrow \infty$ as $\|\mathbf{q}_i - \mathbf{q}_j\| \rightarrow 0$. (iii) $\frac{\partial V_{ij}}{\partial (\|\mathbf{q}_i - \mathbf{q}_j\|)} = 0$ if $\|\mathbf{q}_i - \mathbf{q}_j\| \geq R$. (iv) $V_{ii} = c, i = 1, \dots, n$, where c is a positive constant. 2) If $\|\mathbf{q}_i(0) - \mathbf{q}_j(0)\| < R$, V_{ij} is defined as above except that condition (iii) is replaced with the condition that $V_{ij} \rightarrow \infty$ as $\|\mathbf{q}_i - \mathbf{q}_j\| \rightarrow R$. Based on this potential function, the distributed algorithm is given by

$$\tau_i = \hat{\tau}_i + \mathbf{Y}_i (\mathbf{q}_i, \dot{\mathbf{q}}_i, \hat{\mathbf{v}}_i, \mathbf{v}_i) \hat{\theta}_i, \quad (59)$$

$$\hat{\tau}_i = -\sum_{j=0}^n \frac{\partial V_{ij}}{\partial \mathbf{q}_i} - \gamma \sum_{j=0}^n a_{ij}(t) (\dot{\mathbf{q}}_i - \dot{\mathbf{q}}_j), \quad (60)$$

$$\hat{\mathbf{v}}_i = -\sum_{j=0}^n \frac{\partial V_{ij}}{\partial \dot{\mathbf{q}}_i} - \gamma \sum_{j=0}^n a_{ij}(t) (\dot{\mathbf{q}}_i - \dot{\mathbf{q}}_j), \quad (61)$$

$$\hat{\theta}_i = -\Gamma_i \mathbf{Y}_i^\top (\mathbf{q}_i, \dot{\mathbf{q}}_i, \hat{\mathbf{v}}_i, \mathbf{v}_i) \mathbf{s}_i, \quad (62)$$

where $a_{ij}(t)$ is the weight associated with the proximity graph.

The structure of the above controllers, including (55) and (59) contains two parts, which are constructed based on the fundamental properties of Euler-Lagrange equations. The first part is the coordination feedback term, which drives the states to synchronization. The theoretical analysis is made by designing the Lyapunov function $V = \hat{\mathbf{x}}_i^\top \mathbf{M}_i \hat{\mathbf{x}}_i$ or $V = \hat{\mathbf{q}}_i^\top \mathbf{M}_i^\top \hat{\mathbf{q}}_i$ and the anti-symmetric property of Euler-Lagrange dynamics. The second part is the linear regression, and the parameter adaptive law (58) and (62) are built to deal with the parameter uncertainty of rigid body dynamics.

However, the parameter linearity may not be satisfied for Euler-Lagrange systems with unknown dynamics. A radial basis function neural network (RBFNN) approximation technique is implemented to solve unknown dynamics⁹⁸. The nonlinear dynamics $f(\mathbf{x})$ is modeled as

$$f(\mathbf{x}) = \mathbf{W}^\top \mathbf{H}(\mathbf{x}) + \zeta(\mathbf{x}), \quad \forall \mathbf{x} \in \Omega_{\mathbf{x}}, \quad (63)$$

where $\Omega_{\mathbf{x}}$ is a compact set when RBFNN is used, $\mathbf{W} = [w_1, w_2, \dots, w_l]^\top \in \mathbb{R}^l$ is a weight matrix, l represents the node

number of neural networks, and $\zeta(\mathbf{x})$ is the bounded approximation errors. $\mathbf{H}(\mathbf{x}) = [h_1(\mathbf{x}), h_2(\mathbf{x}), \dots, h_l(\mathbf{x})]^\top$ presents a vector of radial basis function. Then, the coordination controller of Euler-Lagrange system is designed as

$$\tau_i = k_i \mathbf{s}_i - \hat{\mathbf{W}}_i^\top \mathbf{H}_i \quad (64)$$

$$\dot{\hat{\mathbf{W}}}_i = -\gamma (\mathbf{H}_i \mathbf{s}_i^\top + \sigma_i \hat{\mathbf{W}}_i), \quad (65)$$

where $k_i, \gamma, \sigma_i > 0, 0 < \beta_i < 1$. The main difference is the adaptive law (65), which is based on RBFNN approximation. In addition, there are some other approaches, such as robust integral sign of the error strategy⁴⁵ and augmented system method⁹⁹, which are proposed to solve the dynamics uncertainties of Euler-Lagrange systems.

B. Coordination control of multiple rigid body systems on SE(3)

A large amount of results on coordination of Euler-Lagrange systems are based on three fundamental properties of Euler-Lagrange systems in Section 2E. While it may not always be satisfied in some practical applications such as the motion evolving on non-Euclidean manifold and under the external disturbances. The formation control problem on SE(3) is studied with directed and switching topologies⁵⁷. The main idea is to transform the formation problem into the consensus problem of multi-agent systems. Let the state of each agent be described by

$$\mathbf{P}_i(t) = \begin{bmatrix} \mathcal{R}_i(t) & \mathbf{T}_i(t) \\ 0 & 1 \end{bmatrix} \in \mathbb{SE}(3), \quad (66)$$

at each time $t \geq t_0$. The matrix $\mathcal{R}_i(t)$ is an element of SO(3), and the vector $\mathbf{T}_i(t)$ is an element in \mathbb{R}^3 . The relative transformation on SE(3) is given as

$$\begin{aligned} \mathbf{P}_{ij}(t) &= \mathbf{P}_i^{-1}(t) \mathbf{P}_j(t) \\ &= \begin{bmatrix} \mathcal{R}_{ij}(t) & \mathbf{T}_{ij}(t) \\ 0 & 1 \end{bmatrix}, \end{aligned} \quad (67)$$

which contains the relative rotation $\mathcal{R}_{ij}(t) = \mathcal{R}_i^\top(t) \mathcal{R}_j(t)$ and the relative translation $\mathcal{R}_i^\top(t) (\mathbf{T}_j(t) - \mathbf{T}_i(t))$. Let

$$\xi_i = \begin{bmatrix} \omega_i^\wedge & v_i \\ 0 & 0 \end{bmatrix},$$

where ω_i is the angular velocity input and v_i is the transition velocity input. Then, the kinematics of \mathbf{P}_i can be formulated as

$$\dot{\mathbf{P}}_i = \mathbf{P}_i \xi_i. \quad (68)$$

The control goal of the formation is to make $\|\mathbf{P}_i^\top \mathbf{P}_j(t) - \mathbf{P}_{ij}^*\| \rightarrow 0$ as $t \rightarrow \infty$, where \mathbf{P}_{ij}^* is the desired formation pattern. Based on the absolute and relative transformations, the

control protocol can be designed as

$$\xi_i = \sum_{j \in \mathcal{N}_i(t)} a_{ij}(t) \left((\mathbf{P}_j - \mathbf{P}_i) + (\mathbf{P}_i^{-1} - \mathbf{P}_j^{-1}) \right), \quad (69)$$

$$\xi_i = \sum_{j \in \mathcal{N}_i(t)} a_{ij}(t) (\mathbf{P}_{ij} - \mathbf{P}_{ij}^{-1}), \quad (70)$$

respectively. For the absolute transformation case, when using the protocol (69), the formation control can be achieved if each initial rotation is contained in $\mathcal{B}_{\frac{\pi}{2}}(\mathbf{I}_3)$. For the relative transformation case, when using the protocol (70), the formation control can be achieved if all initial rotations are contained in $\mathcal{B}_q(\mathbf{I}_3)$, where $q < \frac{\pi}{4}$. The asymptotic convergence will be achieved by using the protocols (69) and (70). In addition, recalling the knowledge in Section C, we know that the parameterized attitude representation is formulated as $f(\mathcal{R}_i) = g(\theta_i) \mathbf{u}_i(\mathcal{R}_i)$. When the condition $g(\theta_i) > k\theta_i$, $k > 0$ is satisfied, and the topology remains strongly connected for all $t > 0$, a special result of the exponential convergence for the formation control of multiple rigid body systems will be reached where the parameter k determines the exponential rate.

The protocols (69) and (70) are both designed at the kinematic level. A robust formation control on SE(3) is considered with prescribed transit and steady-state performance⁵⁵. The rigid body's motion is modeled by the Euler-Lagrange equation at the dynamic level as follows:

$$\mathbf{M}_i \dot{\mathbf{V}}_i + \mathbf{C}_i(\mathbf{V}_i) \mathbf{V}_i + \mathbf{G}_i(\mathbf{P}_i) + \mathbf{w}_i(\mathbf{P}_i, \mathbf{V}_i, t) = \tau_i, \quad (71)$$

where $\mathbf{P}_i \in \mathbb{SE}(3)$ is defined in (66), $\mathbf{V}_i = [v_i, \omega_i] \in \mathbb{R}^6$, $\mathbf{M}_i \in \mathbb{R}^{6 \times 6}$ is the constant positive definite inertia matrix, $\mathbf{C}_i : \mathbb{R}^6 \rightarrow \mathbb{R}^{6 \times 6}$ is the Coriolis matrix, $\mathbf{G}_i : \mathbb{SE}(3) \rightarrow \mathbb{R}^6$ is the body-frame gravity vector, $\mathbf{w}_i : \mathbb{SE}(3) \times \mathbb{R}^6 \times \mathbb{R}_{\geq 0} \rightarrow \mathbb{R}^6$ is a bounded vector representing model uncertainties and external disturbances, and $\tau_i \in \mathbb{R}^6$ is the control input representing the 6D body-frame generalized force acting on rigid body i . Supposed that the desired formation pattern is specified by $d_{k, \text{des}} \in \mathbb{R}^3$, $\mathcal{R}_{k, \text{des}} \in \text{SO}(3)$, $\forall k \in \mathcal{K}$, the control objective is to design a distributed control input $\tau_i \in \mathbb{R}^6$ such that the following requirements are satisfied $\forall k_1, k_2 \in \mathcal{K}$: 1) $\lim_{t \rightarrow \infty} \|\mathbf{T}_{k_2}(t) - \mathbf{T}_{k_1}(t)\| = d_{k, \text{des}}$; 2) $\lim_{t \rightarrow \infty} [\mathcal{R}_{k_2}(t)]^\top \mathcal{R}_{k_1}(t) = \mathcal{R}_{k, \text{des}}$; 3) $d_{k, \text{col}} < \|\mathbf{T}_{k_2}(t) - \mathbf{T}_{k_1}(t)\| < d_{k, \text{con}}$, $\forall t \in \mathbb{R}$, where $d_{k, \text{col}}$ is the safe distance and $d_{k, \text{con}}$ is the sensing distance between rigid bodies⁵⁵. In addition to the above requirements, there exist constraints of geometric topology of attitude configuration space. To guarantee all control objectives, by transforming the requirements into state constraints, the prescribed performance control is utilized to design the control input of rigid body systems⁵⁵. Note that the desired formation defined by orientation and distance $d_{k, \text{des}} \in \mathbb{R}^3$, $\mathcal{R}_{k, \text{des}} \in \text{SO}(3)$, $\forall k \in \mathcal{K}$ is not guaranteed to be a rigidity formation, which means that the formation cannot be uniquely determined. To solve this problem, the bearing rigidity theory can be utilized to derive the condition that the formation can be uniquely determined up to a transition and inter-neighbor bearings with a scaling factor¹¹⁰. A necessary and sufficient condition for the bearing rigidity is extended

to the manifold such as $\mathbb{SE}(3)$, and the heterogeneous agent dynamics on different manifolds such as \mathbb{S}^1 and $\mathbb{SO}(3)$ are also considered¹¹¹. Based on the bearing rigidity condition, numerous studies have been conducted on the bearing-based formation control for multi-agent systems^{112–115}.

C. Networked coordination control of multiple rigid body systems

The above result assumes that the communication environment is ideal and reliable. The leader-follower consensus problem of networked Euler-Lagrange systems is studied under constrained communication⁵¹. The constrained communication implies that the communication between agents can be intermittent, which is subject to irregular communication time delays and packet dropouts. For each follower $i \in \mathcal{V}_F$, the control input is given by

$$\begin{aligned}\tau_i &= \mathbf{Y}_i \hat{\Theta}_i - k_i^s (\dot{\mathbf{q}}_i - \dot{\mathbf{q}}_{r_i}), \\ \hat{\Theta}_i &= -\Pi_i \mathbf{Y}_i^\top (\dot{\mathbf{q}}_i - \dot{\mathbf{q}}_{r_i}),\end{aligned}\quad (72)$$

where k_i^s is a positive constant and Π_i is a symmetric positive-definite matrix. The reference velocity signal $\dot{\mathbf{q}}_{r_i} \in \mathbb{R}^n$ is designed as follows

$$\begin{bmatrix} \dot{\mathbf{q}}_{r_i} \\ \dot{\hat{\mathbf{v}}}_i \end{bmatrix} = \mathbf{S} \begin{bmatrix} \mathbf{q}_i \\ \hat{\mathbf{v}}_i \end{bmatrix} + \boldsymbol{\eta}_i \quad i \in \mathcal{V}_F, \quad (73)$$

where $\mathbf{S} \in \mathbb{R}^{2n \times 2n}$ is the system matrix of the leader's dynamic model, and $\boldsymbol{\eta}_i \in \mathbb{R}^{2n}$ is an input which is designed as

$$\boldsymbol{\eta}_i = -k_{p_i} (\mathbf{x}_i - \boldsymbol{\varphi}_i) \quad (74)$$

with

$$\dot{\boldsymbol{\varphi}}_i = \mathbf{S} \boldsymbol{\varphi}_i - k_{d_i} (\boldsymbol{\varphi}_i - \boldsymbol{\psi}_i) \quad (75)$$

$$\dot{\boldsymbol{\psi}}_i = \mathbf{S} \boldsymbol{\psi}_i - k_{\psi_i} \left(\boldsymbol{\psi}_i - \frac{1}{\kappa_i} \sum_{j=1}^{n+1} a_{ij} \mathbf{x}_j^* \right), \quad (76)$$

where $\mathbf{x}_i = [\mathbf{q}_i^\top, \hat{\mathbf{v}}_i^\top]^\top$, $k_{p_i}, k_{d_i}, k_{\psi_i} > 0$ are scalar gains, $\kappa_i := \sum_{j=1}^{n+1} a_{ij}$, and

$$\mathbf{x}_{ij}^*(t) := e^{\mathbf{S} \left(t - t_{k_{ij}}^m(t) \right)} \mathbf{x}_j \left(t_{k_{ij}}^m(t) \right), \quad (77)$$

where $\mathbf{x}_j \left(t_{k_{ij}}^m(t) \right)$ is the most recent information of agent $j \in \mathcal{N}_i$ transmitted to agent i . Namely, $\mathbf{x}_{ij}^*(t)$ is the approximation or prediction of the j th agent for i th agent. One of benefits of the above control framework is that it can guarantee the continuity of the control input τ_i . The stability of the above dynamic system (73), (75), and (76) can be shown by using the small gain theorem.

Following the main idea from the above work⁵¹, the consensus problem of networked Euler-Lagrange systems is further studied under jointly connected topologies¹⁰¹. The main

problem is to design the reference velocity input under switching typologies. A high-order dynamic system is constructed in the following form,

$$\dot{\mathbf{x}}_i = (\mathbf{A}_i \otimes \mathbf{I}_m) \mathbf{x}_i + (\mathbf{B}_i \otimes \mathbf{I}_m) \mathbf{u}_i \quad (78)$$

$$\mathbf{y}_i = (\mathbf{C}_i \otimes \mathbf{I}_m) \mathbf{x}_i, \quad (79)$$

where $\mathbf{x}_i \in \mathbb{R}^{km}$, for some $k > 0$, $\mathbf{y}_i \in \mathbb{R}^m$, $\mathbf{A}_i \in \mathbb{R}^{k \times k}$, $\mathbf{B}_i \in \mathbb{R}^k$, and $\mathbf{C}_i \in \mathbb{R}^{1 \times k}$, as well as the input $\mathbf{u}_i \in \mathbb{R}^m$. The high-order system is a high-order filter system where the input \mathbf{u}_i involves the intermittent information transmitted from the switching neighboring agents. Through the filter system, the reference velocity is given by $\mathbf{v}_i \triangleq -\gamma_i (\mathbf{q}_i - \mathbf{y}_i)$, which ensures a continuously differentiable torque input.

Motivated by the limited communication resource in practical application of coordination control of autonomous systems, the research on event-triggered coordination control of multiple rigid body systems has drawn growing attention. The challenging primary lies in introducing the event-triggered sampling in inherent nonlinear rigid body dynamics. The rigid body dynamics are naturally continuous. The event-triggered control turns the closed-loop dynamics into hybrid dynamics, which brings the technical difficulty in revealing the convergence performance. An event-triggered formation control protocol is proposed based on a similar framework in Section 4A, while the event-triggered control is designed based on Barbalat's lemma and small-gain theorem⁵⁴. The sampling-induced errors are regarded as disturbances by using ISS (Input-to-state stability) in the convergence analysis. Another interesting problem is the event-triggered coordination control of multiple rigid body systems under jointly connected topologies. Since the topologies may switch during the inter-event interval, the inconsistency between the protocol and the current topologies should be tackled¹⁰⁴. In addition, the switching topologies also bring additional difficulties in excluding Zeno behavior due to the triggering condition being related to the switching instants¹⁰³.

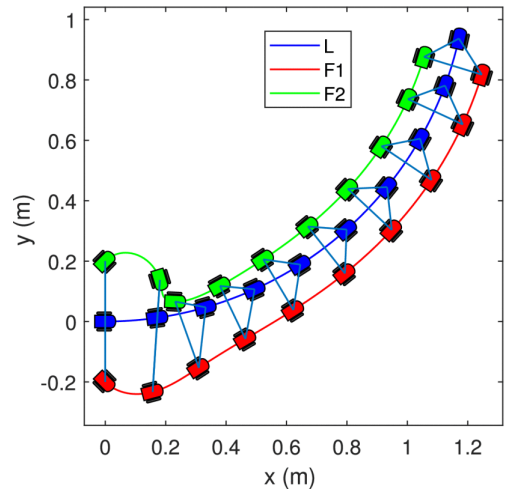


FIG. 5. Formation trajectories of the three agents¹¹⁶.

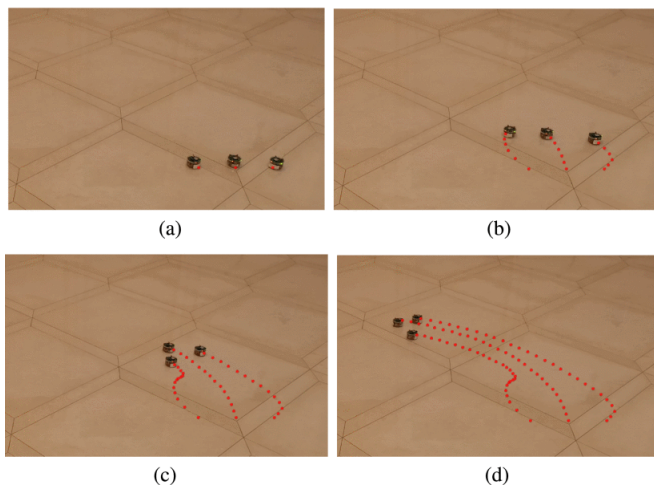


FIG. 6. Experiment snap of formation control for three mobile robots¹¹⁶. (a). $t=0$ s. (b) $t=5$ s. (c) $t=13$ s. (d) $t=26$ s.

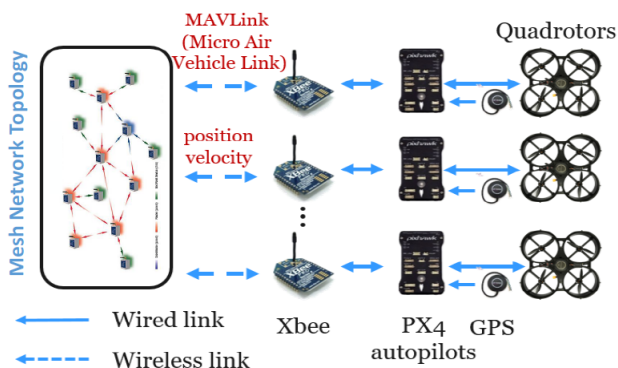


FIG. 7. Experiment platform of formation control for three quadrotors⁵⁴.

D. Experiment results on coordination control of multiple rigid body systems

The coordination control of multiple rigid body systems has wide applications in robotics, transportation, and aerospace. Therefore, researches on practical experiments of coordination control of multiple rigid bodies have been extensively conducted in the literature, including formation control of mobile robots¹¹⁷, unmanned aerial vehicles¹¹⁸, and unmanned surface vehicles¹¹⁹. Here, we only introduce some representative results.

A trajectory tracking and mobile formation coordination on $SE(3)$ is considered for a group of non-holonomic vehicles¹¹⁶. A desired mobile formation control is studied with motion constraints, including weak rigid body motion and strict rigid body motion. The mobile formation under a weak rigid body motion preserves the relative position with the world frame while the mobile formation under a strict rigid body motion preserves the relative position as well as relative attitudes. In Fig. 5, three robots maintain a mobile formation with strict rigid body motion. To show the applicability

of the formation control algorithm, a real experiment using three non-holonomic robots named wheeled E-puck robots is demonstrated¹¹⁶. The communication link among three robots is a directed graph, and the frequency of the communication is 0.1s through blacktooth. The real-time trajectories of three robots in the experiment are shown in Fig. 6. It shows that three robots form a strict rigid body motion similar to the numerical result.

Unmanned aerial vehicles' outdoor formation control is studied in multi-agent frameworks, where a time-varying formation is demonstrated under a switching topology in¹²⁰. In some applications of formation control of unmanned aerial vehicles, the communication resource and energy are limited. An event-triggered formation control is considered for Euler-Lagrange systems⁵⁴. The quadrotor dynamic model is formulated based on the Euler-Lagrange equation. The inner-outer loop control strategy is proposed to achieve the formation control of quadrotors, where the inner loop control is utilized to stabilize the attitude, and the outer loop control guarantees the position and velocity tracking. Thus, to verify the effectiveness of the formation control algorithm, an outdoor formation experiment with three quadrotors is conducted. The flight control experimental system is illustrated in Fig. 7.

The data transmission between quadrotors is built by the DIGI Xbee communication module. The position and velocity information of each quadrotor is obtained by the GPS module. The proposed control algorithm runs on Pixhawk open-source flight controller, which also integrates accelerometers and gyroscope sensors. The experiment result is shown in Fig. 8(a). In the experiment, the communication among quadrotors is governed by an event-triggered broadcasting strategy, which means that each quadrotor only broadcasts its position and velocity information to its neighbor at the triggering instants. The triggering instants are marked by the circle, triangle, and cross in Fig. 8(b). It can be observed that the communication frequency is much reduced compared with the periodic communication strategy.

The last category of practical applications of coordination control is the formation control of unmanned vehicles, including surface vehicles and underwater vehicles. An adaptive formation control of USVs is studied for navigating through narrow channels with unknown curvatures¹²¹. A formation tracking control protocol combing with an unknown water channel curvatures observer is proposed for steering USVs to navigate through irregular narrow channels smoothly. In addition, an experiment result is also conducted based on a multiple USVs control platform which consists of a motion capturing system, a control station, 2.4-GHz wireless modules, and three USVs. The platform is shown in Fig. 9. Three snapshots of the real experiment are shown in Fig. 10, which demonstrates a USV formation traveling along a straight channel segment and an irregular channel segment. It is shown that a flexible formation tracking performance can be achieved with geographical constraints of the winding channel.

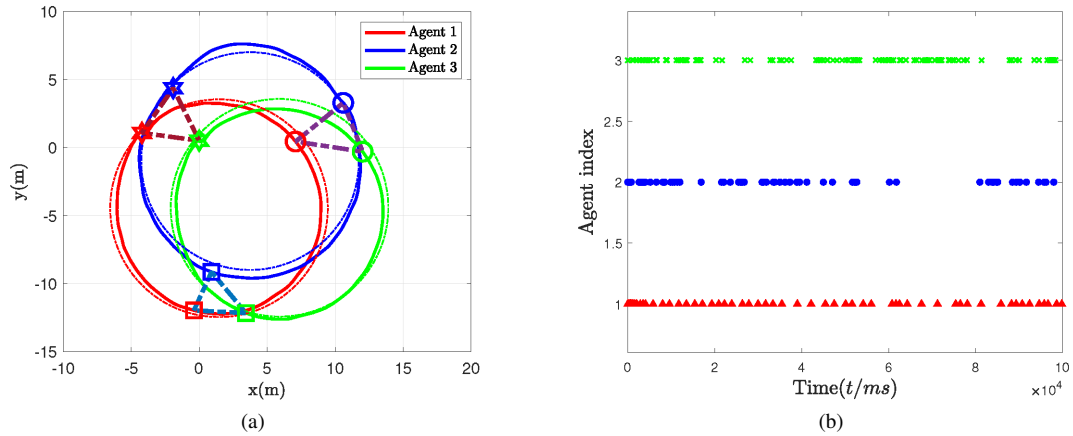


FIG. 8. The experiment results of formation control of multiple quadrotors. (a). Formation trajectories of the three quadrotors. (b). Trigger instants of the three quadrotors⁵⁴.

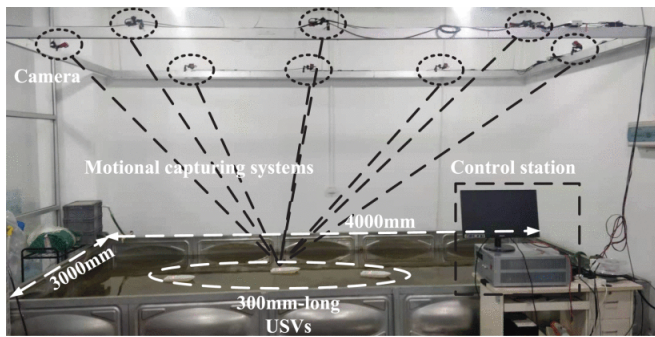


FIG. 9. Multiple USVs control platform¹²¹.

V. CONCLUSION

In this paper, some important topics on synchronization of multiple rigid body systems are surveyed from two aspects. The attitude synchronization problem of multiple rigid body systems is discussed in Section 3, where the main results are divided into local attitude synchronization, global attitude synchronization, and almost global attitude synchronization. More generally, the results of consensus on non-Euclidean spaces such as \mathbb{S}^n and $\mathbb{SO}(n)$ are also discussed. In Section 4, the coordination control of multiple rigid body systems which considers the rotational and translational motion in a unified framework is reviewed. The early works on coordination control of Euler-Lagrange systems are firstly introduced based on the fundamental properties of Euler-Lagrange dynamics. Then, an important topic, which considers the formation control of multiple rigid body systems on $\mathbb{SE}(3)$, and the most recent results on networked coordination control of multiple rigid body systems are discussed. To verify the applicability of proposed coordination algorithms, several experimental results on the formation control of mobile robots, unmanned aerial vehicles, and unmanned surface vehicles are shown, respectively.

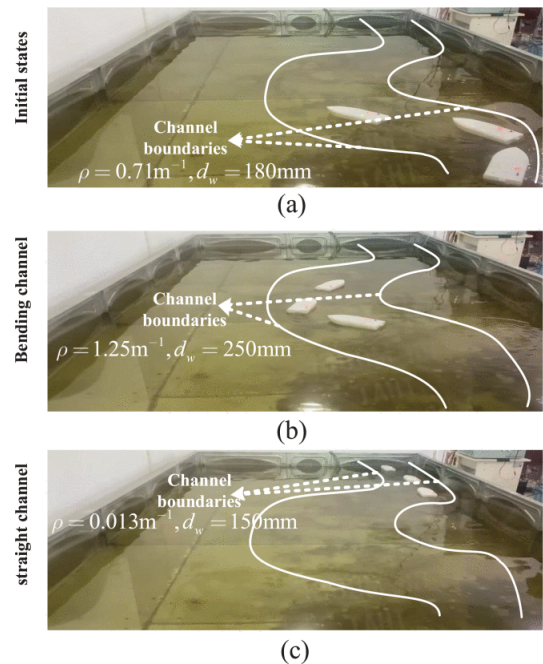


FIG. 10. Experiment snap of formation control for three USVs. (a). Initial states. (b). Bending channel. (c). Straight channel.¹²¹.

In the past few decades, there are much progress in synchronization of multiple rigid body systems. However, there are still some important and challenging issues that should be studied further. Some examples are listed as follows:

- Attitude synchronization with state constraints: There are fewer existing results on attitude synchronization in presence of constraints, which implies that there is unfeasible rotation regions. This problem is highly motivated in the scenarios that the rigid body should avoid lie in certain attitude configurations, such as undesired equilibrium points in the closed-loop dynamics or lim-

ited sensing regions in the aerospace application. Due to the non-Euclidean property of $\mathbb{SO}(3)$, the synchronization protocol with state constraints on $\mathbb{SO}(3)$ is very difficult to be designed.

- Prescribed-time attitude synchronization with absolute and relative attitude measurements: In aerospace applications, the convergence time is an important control index. It is desirable that some space tasks, such as rendezvous and docking of spacecraft, can be completed in a predefined time. However, the existing works of prescribed-time control only focus on linear models. The prescribed-time attitude synchronization, especially only relying on the relative attitude information is still an open problem.
- Coordination control of multiple rigid body systems with communication constraints: The communication network is fundamental for coordination control of multiple rigid body systems. However, in the application of underwater vehicles and spacecraft, the communication among agents is unreliable, and communication capacity is also limited which motivates the study of the coordination control of multiple rigid body systems under communication constraints
- A unified framework of sensing, decision-making, and control of multiple rigid body systems: Most of the existing results consider the control, estimation, and decision-making of multiple rigid body systems separately. However, in practical applications, these processes are generally coupled. The decision-making loop is dependent on the information integrated from environment sensing. The control loop is dependent on the output of the decision-making loop, and is also affected by the estimation error from the sensing loop. Hence, it is necessary to build a unified framework, which can analyze the estimation, decision-making, and control together.
- Experiment researches on the coordination of multiple rigid body systems: Up to our knowledge, the experiment results on coordination control of multiple rigid body systems are quite limited. Most of the researches give the numerical simulation to verify the effectiveness of the proposed algorithm due to the difficulty of real experiments in the extreme environment such as deep spaces. Thus, novel verification approaches such as the semi-physical simulation are one of future directions.

ACKNOWLEDGMENTS

This work was supported by the National Natural Science Foundation of China under Grant No. 62233005, the Young Elite Scientist Sponsorship Program by Cast under Grant No. YESS20220198, the Shanghai Sailing Program under Grant No. 23YF1409600, the Hong Kong Special Administrative Region, China RGC General Research Fund under

Grant CityU 11203521 and Grant CityU 11213023, the Sino-German Center for Research Promotion under Grant M-0066, and the Program of Introducing Talents of Discipline to Universities (the 111 Project) under Grant B17017.

We wish to acknowledge Prof. Jürgen Kurths' many and groundbreaking contributions in the field of nonlinear dynamics, synchronization, and networks, and celebrate Prof. Jürgen Kurths' 70th birthday.

- ¹W. Ren, R. Beard, and E. Atkins, "A survey of consensus problems in multi-agent coordination," in *Proceedings of the 2005, American Control Conference, 2005*. (2005) pp. 1859–1864 vol. 3.
- ²R. Olfati-Saber, J. A. Fax, and R. M. Murray, "Consensus and cooperation in networked multi-agent systems," *Proc. IEEE* **95**, 215–233 (2007).
- ³A. Arenas, A. Díaz-Guilera, J. Kurths, Y. Moreno, and C. Zhou, "Synchronization in complex networks," *Physics Reports* **469**, 93–153 (2008).
- ⁴F. A. Rodrigues, T. K. D. Peron, P. Ji, and J. Kurths, "The kuramoto model in complex networks," *Physics Reports* **610**, 1–98 (2016), the Kuramoto model in complex networks.
- ⁵Y. Tang, J. Kurths, W. Lin, E. Ott, and L. Kocarev, "Introduction to Focus Issue: When machine learning meets complex systems: Networks, chaos, and nonlinear dynamics," *Chaos: An Interdisciplinary Journal of Nonlinear Science* **30** (2020).
- ⁶W. Zhang, D. W. C. Ho, Y. Tang, and Y. Liu, "Quasi-consensus of heterogeneous-switched nonlinear multiagent systems," *IEEE Transactions on Cybernetics* **50**, 3136–3146 (2020).
- ⁷Z. Dayani, F. Parastesh, F. Nazarimehr, K. Rajagopal, S. Jafari, E. Schöll, and J. Kurths, "Optimal time-varying coupling function can enhance synchronization in complex networks," *Chaos: An Interdisciplinary Journal of Nonlinear Science* **33** (2023).
- ⁸W. Ren and R. Beard, *Distributed Consensus in Multi-vehicle Cooperative Control* (Springer London, 2008) pp. 71–82.
- ⁹R. Wei and C. Yongcan, *Distributed coordination of multi-agent networks* (London, 2011).
- ¹⁰S.-J. Chung and J.-J. E. Slotine, "Cooperative robot control and concurrent synchronization of lagrangian systems," *IEEE Transactions on Robotics* **25**, 686–700 (2009).
- ¹¹Y. K. Nakka, W. Hönig, C. Choi, A. Harvard, A. Rahmani, and S.-J. Chung, "Information-based guidance and control architecture for multi-spacecraft on-orbit inspection," *Journal of Guidance, Control, and Dynamics* **45**, 1184–1201 (2022).
- ¹²M. Suresh and D. Ghose, "Uav grouping and coordination tactics for ground attack missions," *IEEE Transactions on Aerospace and Electronic Systems* **48**, 673–692 (2012).
- ¹³C. Zhang, J. Wang, G. G. Yen, C. Zhao, Q. Sun, Y. Tang, F. Qian, and J. Kurths, "When autonomous systems meet accuracy and transferability through ai: A survey," *Patterns* **1**, 100050 (2020).
- ¹⁴Y. Tang, C. Zhao, J. Wang, C. Zhang, Q. Sun, W. X. Zheng, W. Du, F. Qian, and J. Kurths, "Perception and navigation in autonomous systems in the era of learning: A survey," *IEEE Transactions on Neural Networks and Learning Systems*, 1–21 (2022).
- ¹⁵H. Goldstein and J. L. Safko, *Classical Mechanics* (Addison Wesley, 2001).
- ¹⁶T. Chen, J. Shan, and H. Wen, "Distributed adaptive attitude control for networked underactuated flexible spacecraft," *IEEE Transactions on Aerospace and Electronic Systems* **55**, 215–225 (2019).
- ¹⁷X. Jin, Y. Shi, Y. Tang, and X. Wu, "Event-triggered attitude consensus with absolute and relative attitude measurements," *Automatica* **122**, 109245 (2020).
- ¹⁸Z. Meng, W. Ren, and Z. You, "Distributed finite-time attitude containment control for multiple rigid bodies," *Automatica* **46**, 2092–2099 (2010).
- ¹⁹N. Chaturvedi, A. Sanyal, and N. Mcclamroch, "Rigid-body attitude control," *IEEE Control Systems Magazine* **31**, 30–51 (2011).
- ²⁰Y. Tang, H. Gao, W. Zou, and J. Kurths, "Distributed synchronization in networks of agent systems with nonlinearities and random switchings," *IEEE Trans. Cybern.* **43**, 358–370 (2013).
- ²¹M. Shuster, "A survey of attitude representations," *The Journal of the Astronautical Sciences* **41**, 439–517 (1993).
- ²²W. Ren, "Distributed cooperative attitude synchronization and tracking for

- multiple rigid bodies,” *IEEE Transactions on Control Systems Technology* **18**, 383–392 (2010).
- ²³C. Mayhew, R. Sanfelice, J. Sheng, M. Arcak, and A. Teel, “Quaternion-based hybrid feedback for robust global attitude synchronization,” *IEEE Transactions on Automatic Control* **57**, 2122–2127 (2012).
- ²⁴A. Sarlette, R. Sepulchre, and N. E. Leonard, “Autonomous rigid body attitude synchronization,” *Automatica* **45**, 572–577 (2009).
- ²⁵Y. Igarashi, T. Hatanaka, M. Fujita, and M. W. Spong, “Passivity-based attitude synchronization in $se(3)$,” *IEEE Transactions on Control Systems Technology* **17**, 1119–1134 (2009).
- ²⁶Y. Zou and Z. Meng, “Velocity-free leader–follower cooperative attitude tracking of multiple rigid bodies on $so(3)$,” *IEEE Transactions on Cybernetics* **49**, 4078–4089 (2019).
- ²⁷S. P. Bhat and D. S. Bernstein, “A topological obstruction to continuous global stabilization of rotational motion and the unwinding phenomenon,” *Systems & Control Letters* **39**, 63–70 (2000).
- ²⁸J. Thunberg, W. Song, E. Montijano, Y. Hong, and X. Hu, “Distributed attitude synchronization control of multi-agent systems with switching topologies,” *Automatica* **50**, 832–840 (2014).
- ²⁹J. Markdahl, J. Thunberg, and J. Gonçalves, “Almost global consensus on the n -sphere,” *IEEE Transactions on Automatic Control* **63**, 1664–1675 (2018).
- ³⁰P. O. Pereira and D. V. Dimarogonas, “Family of controllers for attitude synchronization on the sphere,” *Automatica* **75**, 271–281 (2017).
- ³¹P. O. Pereira, D. Boskos, and D. V. Dimarogonas, “A common framework for complete and incomplete attitude synchronization in networks with switching topology,” *IEEE Transactions on Automatic Control* **65**, 271–278 (2020).
- ³²E. Montbrío, J. Kurths, and B. Blasius, “Synchronization of two interacting populations of oscillators,” *Phys. Rev. E* **70**, 056125 (2004).
- ³³N. Fujiwara, J. Kurths, and A. Díaz-Guilera, “Synchronization in networks of mobile oscillators,” *Phys. Rev. E* **83**, 025101 (2011).
- ³⁴S. Rakshit, S. Majhi, J. Kurths, and D. Ghosh, “Neuronal synchronization in long-range time-varying networks,” *Chaos: An Interdisciplinary Journal of Nonlinear Science* **31** (2021).
- ³⁵Q. Li, H. Chen, Y. Li, M. Feng, and J. Kurths, “Network spreading among areas: A dynamical complex network modeling approach,” *Chaos: An Interdisciplinary Journal of Nonlinear Science* **32** (2022).
- ³⁶P. Ji, J. Ye, Y. Mu, W. Lin, Y. Tian, C. Hens, M. Perc, Y. Tang, J. Sun, and J. Kurths, “Signal propagation in complex networks,” *Physics Reports* **1017**, 1–96 (2023), signal propagation in complex networks.
- ³⁷L. Mazzearella, A. Sarlette, and F. Ticozzi, “Consensus for Quantum Networks: Symmetry from Gossip Interactions,” *IEEE Transactions on Automatic Control* **60**, 158–172 (2015).
- ³⁸G. Shi, D. Dong, S. Member, I. R. Petersen, and K. H. Johansson, “Reaching a Quantum Consensus : Master Equations That Generate Symmetrization and Synchronization,” *IEEE Transactions on Automatic Control* **61**, 374–387 (2016).
- ³⁹G. Shi, S. Fu, I. R. Petersen, and A. Q. States, “Consensus of Quantum Networks With Directed Interactions : Fixed and Switching Structures,” *IEEE Transactions on Automatic Control* **62**, 2014–2019 (2017).
- ⁴⁰R. Sepulchre, “Consensus on nonlinear spaces,” *Annual Reviews in Control* **35**, 56–64 (2011).
- ⁴¹J. Markdahl, “Synchronization on riemannian manifolds: Multiply connected implies multistable,” *IEEE Transactions on Automatic Control* **66**, 4311–4318 (2021).
- ⁴²J. Markdahl, J. Thunberg, and J. Gonçalves, “High-dimensional kuramoto models on stiefel manifolds synchronize complex networks almost globally,” *Automatica* **113**, 108736 (2020).
- ⁴³J. Thunberg, J. Markdahl, F. Bernard, and J. Gonçalves, “Lifting method for analyzing distributed synchronization on the unit sphere,” *Automatica* **96**, 253–258 (2018).
- ⁴⁴J. Thunberg, J. Markdahl, and J. Gonçalves, “Dynamic controllers for column synchronization of rotation matrices: A qr-factorization approach,” *Automatica* (2018).
- ⁴⁵J. R. Klotz, Z. Kan, J. M. Shea, E. L. Pasilio, and W. E. Dixon, “Asymptotic synchronization of a leader-follower network of uncertain euler-lagrange systems,” *IEEE Transactions on Control of Network Systems* **2**, 174–182 (2015).
- ⁴⁶W. Ren, “Distributed leaderless consensus algorithms for networked Euler-Lagrange systems,” *Int. J. Control* **82**, 2137–2149 (2009).
- ⁴⁷H. Wang, “Flocking of networked uncertain euler-lagrange systems on directed graphs,” *Automatica* **49**, 2774–2779 (2013).
- ⁴⁸C. Liu and N. Chopra, “Controlled synchronization of heterogeneous robotic manipulators in the task space,” *IEEE Transactions on Robotics* **28**, 268–275 (2012).
- ⁴⁹H. Wang, “Consensus of networked mechanical systems with communication delays: A unified framework,” *IEEE Transactions on Automatic Control* **59**, 1571–1576 (2014).
- ⁵⁰A. Abdessameud, I. G. Polushin, and A. Tayebi, “Synchronization of lagrangian systems with irregular communication delays,” *IEEE Transactions on Automatic Control* **59**, 187–193 (2014).
- ⁵¹A. Abdessameud, A. Tayebi, and I. Polushin, “Leader-follower synchronization of Euler-Lagrange systems with time-varying leader trajectory and constrained discrete-time communication,” *IEEE Transactions on Automatic Control* **62**, 2539–2545 (2017).
- ⁵²W. Zhang, Y. Tang, T. Huang, and A. Vasilakos, “Consensus of networked Euler-Lagrange systems under time-varying sampled-data control,” **14**, 535–544 (2018).
- ⁵³X. Jin, W. Du, W. He, L. Kocarev, Y. Tang, and J. Kurths, “Twisting-based finite-time consensus for Euler-Lagrange systems with an event-triggered strategy,” *IEEE Transactions on Network Science and Engineering* **7**, 1007–1018 (2020).
- ⁵⁴X. Jin, Y. Tang, Y. Shi, W. Zhang, and W. Du, “Event-triggered formation control for a class of uncertain euler-lagrange systems: Theory and experiment,” *IEEE Transactions on Control Systems Technology* **30**, 336–343 (2022).
- ⁵⁵C. K. Verginis, A. Nikou, and D. V. Dimarogonas, “Robust formation control in $se(3)$ for tree-graph structures with prescribed transient and steady state performance,” *Automatica* **103**, 538–548 (2019).
- ⁵⁶T. Hatanaka, Y. Igarashi, M. Fujita, and M. W. Spong, “Passivity-based pose synchronization in three dimensions,” *IEEE Transactions on Automatic Control* **57**, 360–375 (2012).
- ⁵⁷J. Thunberg, X. Hu, and J. Gonçalves, “Consensus and formation control on $SE(3)$ for switching topologies,” *Automatica* **66**, 63–82 (2016).
- ⁵⁸T. Chen, J. Shan, H. Wen, and S. Xu, “Review of attitude consensus of multiple spacecraft,” *Astrodynamics* **6**, 329–356 (2022).
- ⁵⁹H. Cai and J. Huang, “Leader-following attitude consensus of multiple rigid body systems by attitude feedback control,” *Automatica* **69**, 87–92 (2016).
- ⁶⁰F. Hadaegh and R. Smith, “Control topologies for deep space formation flying spacecraft,” *Journal of Guidance, Control and Dynamics* **28**, 106–114 (2005).
- ⁶¹X. Jin, Y. Shi, Y. Tang, H. Werner, and J. Kurths, “Event-triggered fixed-time attitude consensus with fixed and switching topologies,” *IEEE Transactions on Automatic Control* **67**, 4138–4145 (2022).
- ⁶²I. Bayezit and B. Fidan, “Distributed cohesive motion control of flight vehicle formations,” *IEEE Transactions on Industrial Electronics* **60**, 5763–5772 (2013).
- ⁶³D. V. Dimarogonas, P. Tsiotras, and K. J. Kyriakopoulos, “Leader–follower cooperative attitude control of multiple rigid bodies,” *Systems & Control Letters* **58**, 429–435 (2009).
- ⁶⁴Y. Tang, X. Jin, Y. Shi, and W. Du, “Event-triggered attitude synchronization of multiple rigid body systems with velocity-free measurements,” *Automatica* , 143 (2022).
- ⁶⁵T. Liu and J. Huang, “Leader-following attitude consensus of multiple rigid body systems subject to jointly connected switching networks,” *Automatica* **92**, 63–71 (2018).
- ⁶⁶C. He and J. Huang, “Leader-following consensus of multiple rigid body systems by a sampled-data distributed observer,” *AUTOMATICA* **146** (2022).
- ⁶⁷H. Gui and A. H. de Ruiter, “Global finite-time attitude consensus of leader-following spacecraft systems based on distributed observers,” *Automatica* **91**, 225–232 (2018).
- ⁶⁸Y. Tang, D. Zhang, X. Jin, D. Yao, and F. Qian, “A resilient attitude tracking algorithm for mechanical systems,” *IEEE/ASME Transactions on Mechatronics* **24**, 2550–2561 (2019).
- ⁶⁹D. Zhang, Y. Tang, X. Jin, and J. Kurths, “Quaternion-based attitude synchronization with an event-based communication strategy,” *IEEE Transactions on Circuits and Systems I: Regular Papers* **69**, 1333–1346 (2022).

- ⁷⁰Y. Zou, Z. Zhou, X. Dong, and Z. Meng, "Distributed formation control for multiple vertical takeoff and landing uavs with switching topologies," *IEEE/ASME Transactions on Mechatronics* **23**, 1750–1761 (2018).
- ⁷¹R. Tron, B. Afsari, and R. Vidal, "Riemannian consensus for manifolds with bounded curvature," *IEEE Transactions on Automatic Control* **58**, 921–934 (2013).
- ⁷²X. Jin, S. Mao, L. Kocarev, C. Liang, S. Wang, and Y. Tang, "Event-triggered optimal attitude consensus of multiple rigid body networks with unknown dynamics," *IEEE Transactions on Network Science and Engineering* **9**, 3701–3714 (2022).
- ⁷³C. Xu, B. Wu, and D. Wang, "Distributed prescribed-time attitude coordination for multiple spacecraft with actuator saturation under directed graph," *IEEE Transactions on Aerospace and Electronic Systems* **58**, 2660–2672 (2022).
- ⁷⁴A. Abdessameud, A. Tayebi, and I. Polushin, "Attitude synchronization of multiple rigid bodies with communication delays," *IEEE Transactions on Automatic Control* **57**, 2405–2411 (2012).
- ⁷⁵Y. Tang, D. Zhang, X. Jin, D. Yao, and F. Qian, "A resilient attitude tracking algorithm for mechanical systems," *IEEE/ASME Transactions on Mechatronics* **24**, 2550–2561 (2019).
- ⁷⁶S. Berkane, A. Abdessameud, and A. Tayebi, "Hybrid global exponential stabilization on $so(3)$," *Automatica* **81**, 279–285 (2017).
- ⁷⁷M. Wang and A. Tayebi, "Hybrid feedback for global tracking on matrix lie groups $so(3)$ and $se(3)$," *IEEE Transactions on Automatic Control* **67**, 2930–2945 (2022).
- ⁷⁸S. Berkane, A. Abdessameud, and A. Tayebi, "Hybrid output feedback for attitude tracking on $\mathbb{S}O(3)$," *IEEE Transactions on Automatic Control* **63**, 3956–3963 (2018).
- ⁷⁹B. Afsari, "Riemannian L^p center of mass: existence, uniqueness, and convexity," *Proceedings of the American Mathematical Society* **139**, 655–673 (2014).
- ⁸⁰J. Wei, S. Zhang, A. Adaldo, J. Thunberg, X. Hu, and K. Johansson, "Finite-time attitude synchronization with distributed discontinuous protocols," *IEEE Transactions on Automatic Control* **63**, 3608–3615 (2018).
- ⁸¹M. G. Rosenblum, A. S. Pikovsky, and J. Kurths, "Phase synchronization of chaotic oscillators," *Phys. Rev. Lett.* **76**, 1804–1807 (1996).
- ⁸²M. G. Rosenblum, A. S. Pikovsky, and J. Kurths, "From phase to lag synchronization in coupled chaotic oscillators," *Phys. Rev. Lett.* **78**, 4193–4196 (1997).
- ⁸³V. Godavarthi, P. Kasthuri, S. Mondal, R. I. Sujith, N. Marwan, and J. Kurths, "Synchronization transition from chaos to limit cycle oscillations when a locally coupled chaotic oscillator grid is coupled globally to another chaotic oscillator," *Chaos: An Interdisciplinary Journal of Nonlinear Science* **30** (2020).
- ⁸⁴J. Markdahl, J. Thunberg, and J. Goncalves, "High-dimensional kuramoto models on stiefel manifolds synchronize complex networks almost globally," *Automatica* **113**, 108736 (2020).
- ⁸⁵H. Du and S. Li, "Attitude synchronization for flexible spacecraft with communication delays," *IEEE Transactions on Automatic Control* **61**, 3625–3630 (2016).
- ⁸⁶M. Feng, S. Deng, F. Chen, and J. Kurths, "Distributed event-triggered adaptive partial diffusion strategy under dynamic network topology," *Chaos: An Interdisciplinary Journal of Nonlinear Science* **30** (2020).
- ⁸⁷X. Li, Z. Sun, Y. Tang, and H. R. Karimi, "Adaptive event-triggered consensus of multiagent systems on directed graphs," *IEEE Transactions on Automatic Control* **66**, 1670–1685 (2021).
- ⁸⁸X. Li, Y. Tang, and H. R. Karimi, "Consensus of multi-agent systems via fully distributed event-triggered control," *Automatica* **116**, 108898 (2020).
- ⁸⁹Y. Tang, D. Zhang, P. Shi, W. Zhang, and F. Qian, "Event-based formation control for nonlinear multiagent systems under dos attacks," *IEEE Transactions on Automatic Control* **66**, 452–459 (2021).
- ⁹⁰W. Xu, D. W. C. Ho, L. Li, and J. Cao, "Event-triggered schemes on leader-following consensus of general linear multiagent systems under different topologies," *IEEE Transactions on Cybernetics* **47**, 212–223 (2017).
- ⁹¹S. Du, W. Xu, J. Qiao, and D. W. C. Ho, "Resilient output synchronization of heterogeneous multiagent systems with dos attacks under distributed event-/self-triggered control," *IEEE Transactions on Neural Networks and Learning Systems* **34**, 1169–1178 (2023).
- ⁹²W. Xu, W. He, D. W. Ho, and J. Kurths, "Fully distributed observer-based consensus protocol: Adaptive dynamic event-triggered schemes," *Automatica* **139**, 110188 (2022).
- ⁹³X. Xie, T. Sheng, and L. He, "Distributed event-triggered attitude consensus control for spacecraft formation flying with unknown disturbances and uncertainties," *IEEE Transactions on Aerospace and Electronic Systems* **58**, 1721–1732 (2022).
- ⁹⁴J. Mei, W. Ren, and G. Ma, "Distributed coordinated tracking with a dynamic leader for multiple Euler-Lagrange systems," *IEEE Transactions on Automatic Control* **56**, 1415–1421 (2011).
- ⁹⁵J. Mei, W. Ren, and G. Ma, "Distributed containment control for lagrangian networks with parametric uncertainties under a directed graph," *Automatica* **48**, 653–659 (2012).
- ⁹⁶W. Zhang, Y. Tang, T. Huang, and A. Vasilakos, "Consensus of networked Euler-Lagrange systems under time-varying sampled-data control," *IEEE Transactions on Industrial Informatics* **14**, 535–544 (2018).
- ⁹⁷T. Xu, Y. Hao, and Z. Duan, "Fully distributed containment control for multiple euler-lagrange systems over directed graphs: An event-triggered approach," *IEEE Transactions on Circuits and Systems I: Regular Papers* **67**, 2078–2090 (2020).
- ⁹⁸Y. Shi, Q. Hu, X. Shao, and Y. Shi, "Adaptive neural coordinated control for multiple euler-lagrange systems with periodic event-triggered sampling," *IEEE Transactions on Neural Networks and Learning Systems* , 1–11 (2022).
- ⁹⁹S. Wang, X. Jin, S. Mao, A. V. Vasilakos, and Y. Tang, "Model-free event-triggered optimal consensus control of multiple euler-lagrange systems via reinforcement learning," *IEEE Transactions on Network Science and Engineering* **8**, 246–258 (2021).
- ¹⁰⁰B. Wei, F. Xiao, F. Fang, and Y. Shi, "Velocity-free event-triggered control for multiple euler-lagrange systems with communication time delays," *IEEE Transactions on Automatic Control* **66**, 5599–5605 (2021).
- ¹⁰¹A. Abdessameud, "Consensus of nonidentical Euler-Lagrange systems under switching directed graphs," *IEEE Transactions on Automatic Control* **64**, 2108–2114 (2019).
- ¹⁰²C. He and J. Huang, "Leader-following consensus for a class of multiple robot manipulators over switching networks by distributed position feedback control," *IEEE Transactions on Automatic Control* **65**, 890–896 (2020).
- ¹⁰³W. Hu, L. Liu, and G. Feng, "Event-triggered cooperative output regulation of linear multi-agent systems under jointly connected topologies," *IEEE Transactions on Automatic Control* **64**, 1317–1322 (2019).
- ¹⁰⁴Y. Hao, J. Zhang, and L. Liu, "Fully distributed event-triggered cooperative output regulation of multi-agent systems under jointly connected digraphs," *IEEE Transactions on Automatic Control* , 1–8 (2022).
- ¹⁰⁵A. Girard, "Dynamic triggering mechanisms for event-triggered control," *IEEE Transactions on Automatic Control* **60**, 1992–1997 (2015).
- ¹⁰⁶D. Zhang, Y. Tang, W. Zhang, and X. Wu, "Hierarchical design for position-based formation control of rotorcraft-like aerial vehicles," *IEEE Transactions on Control of Network Systems* **7**, 1789–1800 (2020).
- ¹⁰⁷S.-J. Chung, "Application of synchronization to formation flying spacecraft: Lagrangian approach," *Journal of Guidance, Control, and Dynamics* **32** (2009).
- ¹⁰⁸S. Wang, X. Jin, S. Mao, A. V. Vasilakos, and Y. Tang, "Model-free event-triggered optimal consensus control of multiple euler-lagrange systems via reinforcement learning," *IEEE Transactions on Network Science and Engineering* **8**, 246–258 (2021).
- ¹⁰⁹S. Ghabani, J. Mei, W. Ren, and Y. Song, "Fully distributed flocking with a moving leader for lagrange networks with parametric uncertainties," *Automatica* **67**, 67–76 (2016).
- ¹¹⁰M. H. Trinh, Q. Van Tran, and H.-S. Ahn, "Minimal and redundant bearing rigidity: Conditions and applications," *IEEE Transactions on Automatic Control* **65**, 4186–4200 (2020).
- ¹¹¹G. Michieletto, A. Cenedese, and D. Zelazo, "A unified dissertation on bearing rigidity theory," *IEEE Transactions on Control of Network Systems* **8**, 1624–1636 (2021).
- ¹¹²S. Zhao and D. Zelazo, "Bearing rigidity and almost global bearing-only formation stabilization," *IEEE Transactions on Automatic Control* **61**, 1255–1268 (2016).
- ¹¹³L. Chen and M. Cao, "Angle rigidity for multi-agent formations in 3d," *IEEE Transactions on Automatic Control* , 1–16 (2023).
- ¹¹⁴M. H. Trinh, S. Zhao, Z. Sun, D. Zelazo, B. D. O. Anderson, and H.-S. Ahn, "Bearing-based formation control of a group of agents with leader-

- first follower structure,” *IEEE Transactions on Automatic Control* **64**, 598–613 (2019).
- ¹¹⁵S. Zhao and D. Zelazo, “Translational and scaling formation maneuver control via a bearing-based approach,” *IEEE Transactions on Control of Network Systems* **4**, 429–438 (2017).
- ¹¹⁶X. Peng, Z. Sun, K. Guo, and Z. Geng, “Mobile formation coordination and tracking control for multiple nonholonomic vehicles,” *IEEE/ASME Transactions on Mechatronics* **25**, 1231–1242 (2020).
- ¹¹⁷L. A. Valbuena Reyes and H. G. Tanner, “Flocking, formation control, and path following for a group of mobile robots,” *IEEE Transactions on Control Systems Technology* **23**, 1268–1282 (2015).
- ¹¹⁸X. Dong, B. Yu, Z. Shi, and Y. Zhong, “Time-varying formation control for unmanned aerial vehicles: theories and applications,” *IEEE Transactions on Control System Technology* **23**, 340–348 (2015).
- ¹¹⁹Z. Peng, J. Wang, D. Wang, and Q.-L. Han, “An overview of recent advances in coordinated control of multiple autonomous surface vehicles,” *IEEE Transactions on Industrial Informatics* **17**, 732–745 (2021).
- ¹²⁰X. Dong, Y. Zhou, Z. Ren, and Y. Zhong, “Time-varying formation tracking for second-order multi-agent systems subjected to switching topologies with application to quadrotor formation flying,” *IEEE Transactions on Industrial Electronics* **64**, 5014–5024 (2017).
- ¹²¹C. Tang, H.-T. Zhang, and J. Wang, “Flexible formation tracking control of multiple unmanned surface vessels for navigating through narrow channels with unknown curvatures,” *IEEE Transactions on Industrial Electronics* **70**, 2927–2938 (2023).